LIMNOLOGY AND OCEANOGRAPHY ASLO Association for the Sciences of Limnology and Oceanography

Attenuation of photosynthetically active radiation and ultraviolet light in response to changing dissolved organic carbon in browning lakes: Modelling and parametrization

Journal:	*Limnology and Oceanography*
Manuscript ID	LO-20-0366.R2
Wiley - Manuscript type:	Original Article
Date Submitted by the Author:	n/a
Complete List of Authors:	Pilla, Rachel; Miami University, Department of Biology Couture, Raoul; Université Laval, Centre for Northern Studies (CEN), Takuvik Joint International Laboratory, and Department of Chemistry
Keywords:	process-based model, light attenuation, dissolved organic carbon, photosynthetically active radiation, ultraviolet radiation, lake browning
Abstract:	We present and evaluate an update to the process-based lake model MyLake that includes a time-varying linkage between light attenuation of both photosynthetically active radiation (PAR) and ultraviolet (UV) wavelengths to changes in dissolved organic carbon (DOC). In many parts of northeastern North America and Europe, DOC in lakes has rapidly increased, leading to reduced water transparency and increases in light attenuation. These changes alter the vertical light and heat distribution that affect vertical structuring of temperature and dissolved oxygen. We use this model update to test the responsiveness of PAR and UV attenuation to short-term fluctuations in DOC and with a test case of long-term browning at Lake Giles (Pennsylvania, USA). Lake Giles has browned significantly since the late 1980s, and three decades of detailed empirical data have indicated more than a doubling of DOC concentrations, and consequent increases in PAR and UV light attenuation, warming surface waters, cooling deep waters, and increasing deepwater oxygen depletion. We found that the model performance improves by 16% and 52% for long-term trends in PAR and UV attenuation, respectively, when these coefficients respond directly to in-lake DOC concentrations. Further, long-term trends in surface water warming, deepwater cooling, and deepwater oxygen depletion in Lake Giles were better captured by the model following this update, and were very rapid due to its high water transparency and low DOC. Hence, incorporating a responsive link between DOC and light attenuation in lake models is key to understanding long-term lake browning patterns, mechanisms, and ecological consequences.

Scientific Significance Statement Topic

Widespread decreases in water transparency in lakes due to browning fundamentally modify the vertical light and heat distribution. In turn, thermal and chemical gradients shaping the lake ecosystem are altered, with numerous consequences for habitat availability and trophic interactions. These changes can threaten ecosystem functioning and services that are vital to freshwater drinking quality. However, long-term empirical data sets with physical, chemical, and biological variables in lakes experiencing browning are incredibly rare; here, ecosystem modelling can give insights into the likely ecological responses to browning as well as partitioning key mechanisms. In most lake models, light attenuation has been treated as a static variable for a single wavelength (e.g., 320 nm ultraviolet radiation) or waveband (e.g., photosynthetically active radiation, PAR). Here, in contrast, we test a model formulation that includes both PAR and ultraviolet wavelengths and we predict their dynamic response to long-term browning driven by increases in dissolved organic carbon. Explicitly accounting for multiple wavelengths is important for improving accuracy and more fully understanding the range of possible ecosystem consequences of browning that are currently poorly understood.

Scientific Significance Statement Outlet

This research encapsulates physical, chemical, and biological implications for lake ecosystems experiencing changes in water transparency, and incorporates long-term empirical data, high-frequency sensor data, and updated modelling work in a single study. Hence, Limnology & Oceanography is uniquely fitted for its publication as a novel modelling approach to a regional to global scale issue facing both freshwater and marine systems.

Title:

Attenuation of photosynthetically active radiation and ultraviolet light in response to changing dissolved organic carbon in browning lakes: Modelling and parametrization

Authors & Affiliations:

Rachel M. Pilla[1*] (pillarm@miamioh.edu; ORCID 0000-0001-9156-9486)

Raoul-Marie Couture[2] (raoul.couture@chm.ulaval.ca; ORCID 0000-0003-4940-3372)

[1]Department of Biology, Miami University, Oxford, Ohio, USA

[2]Centre for Northern Studies (CEN), Takuvik Joint International Laboratory, and Department of Chemistry, Université Laval, Quebec City, QC, Canada

[*]corresponding author

Running Head:

Modelling light attenuation in browning lakes

Keywords/Search Terms:

process-based model, light attenuation, dissolved organic carbon, photosynthetically active radiation, ultraviolet light, lake browning

Abstract:

We present and evaluate an update to the process-based lake model MyLake that includes a time-varying linkage between light attenuation of both photosynthetically active radiation (PAR) and ultraviolet (UV) wavelengths to changes in dissolved organic carbon (DOC). In many parts of northeastern North America and Europe, DOC in lakes has rapidly increased, leading to reduced water transparency and increases in light attenuation. These changes alter the vertical light and heat distribution that affect vertical structuring of temperature and dissolved oxygen. We use this model update to test the responsiveness of PAR and UV attenuation to short-term fluctuations in DOC and with a test case of long-term browning at Lake Giles (Pennsylvania, USA). Lake Giles has browned significantly since the late 1980s, and three decades of detailed empirical data have indicated more than a doubling of DOC concentrations, and consequent increases in PAR and UV light attenuation, warming surface waters, cooling deep waters, and increasing deepwater oxygen depletion. We found that the model performance improves by 16% and 52% for long-term trends in PAR and UV attenuation, respectively, when these coefficients respond directly to in-lake DOC concentrations. Further, long-term trends in surface water warming, deepwater cooling, and deepwater oxygen depletion in Lake Giles were better captured by the model following this update, and were very rapid due to its high water transparency and low DOC. Hence, incorporating a responsive link between DOC and light attenuation in lake models is key to understanding long-term lake browning patterns, mechanisms, and ecological consequences.

Introduction:

In northern boreal lakes, decreases in water transparency have been one of the most widespread responses to anthropogenic stressors in recent decades. The most prevalent driver of decreasing water transparency in lakes in northeastern North America and northern Europe is an increase in terrestrially-derived dissolved organic carbon (DOC; Evans et al. 2006; Monteith et al. 2007). Termed "browning" (Roulet and Moore 2006), increases in DOC in lakes have been attributed to (1) recovery from anthropogenic acidification (Evans et al. 2006; Monteith et al. 2007; Strock et al. 2014), (2) increases in precipitation and extreme storm events (Zhang et al. 2010; de Wit et al. 2016; Williamson et al. 2016), and (3) permafrost thaw (Wauthy et al. 2018). These increases in DOC lead to increased light attenuation of both photosynthetically active radiation (PAR) and ultraviolet (UV) radiation (Williamson et al. 2015) and interactively result in important ecosystem change, such as increased production of reactive oxygen species in surface waters (Wolf et al. 2018) that can, in turn, negatively influence aquatic biota (Cooke et al. 2003; Paerl and Otten 2013; Wolf et al. 2017).

Changes in attenuation of PAR affect the vertical heat distribution in the water column and therefore the lake thermal structure (Read and Rose 2013; Rose et al. 2016; Pilla et al. 2018). Decreasing water transparency and consequent increases in thermal stability further influence other physio-chemical properties of lakes, such as hindered gas solubility/diffusion and faster metabolic rates, both responsible for deepwater dissolved oxygen depletion (Brothers et al. 2014; Knoll et al. 2018). These and other responses, such as the selectively increased attenuation of UV radiation (Williamson et al. 1996), are important to understanding the full array of biological and ecological responses in lake ecosystems experiencing browning (Solomon et al. 2015).

It is well-documented that light attenuation, and thus water transparency, is strongly driven by DOC concentration and DOC-specific absorption, also referred to as DOC optical cross-section (Morris et al. 1995; Williamson et al. 1996; Pace and Cole 2002). However, very few long-term empirical datasets exist that document detailed measurements of these variables in lakes experiencing browning, in addition to the associated long-term physical, biological, and ecological responses (Williamson et al. 2015). Hence, models can be used to understand and expand upon the long-term changes in lakes experiencing browning (Couture et al. 2015; Kiuru et al. 2019). Further, in conjunction with long-term empirical data, modelling studies can be used to support casual linkages between browning-related drivers and ecological responses, whereas in empirical studies alone, assigning direct causality is otherwise difficult without paired experimental evidence (Williamson et al. 2015; Pilla et al. 2018). Presumably owing in part to the lack of relevant time-series, no process-based lake ecosystem models currently include time-varying light attenuation of both PAR and UV wavelengths, which are key structural and ecological variables for a variety of chemical processes (Cory et al. 2014) and biological responses (Williamson et al. 1999; Overholt et al. 2012; Hansen et al. 2019).

Attenuation of UV light is highly responsive to changes in DOC and water transparency, often more so that PAR attenuation due to the selective absorption of UV wavelengths by DOC compared to PAR wavelengths (Williamson et al. 1996). The ecological responses to decreased UV penetration may result in improved survival of UV-sensitive zooplankton or young-of-year fish (Williamson et al. 1999), but may also increase the risk of parasites and pathogen spread (Overholt et al. 2012; Williamson et al. 2017). However, most lake ecosystem models currently lack a time-varying pairing between DOC and PAR light attenuation. Such pairing between DOC concentration and light attenuation would allow these two state variables to vary as a function of time in response to both changing external DOC loads and *in-situ* DOC processing via photobleaching, metabolism, and flocculation. Further, models do not currently include UV attenuation as a response to increasing DOC, which is a key component of modelling the array of ecosystem responses to long-term lake browning.

To model lake browning, we updated the one-dimensional process-based lake model MyLake (Saloranta and Andersen 2007) to include and test an explicit, time-varying linkage between DOC concentration and attenuation of both PAR and UV wavelengths. First, we tested the responsiveness of modeled PAR and UV attenuation to seasonal fluctuations in DOC loads. Second, we tested model performance in a long-term browning scenario at Lake Giles (Pennsylvania, USA; Fig. 1). We integrated empirical data from Lake Giles, which has experienced marked browning in the past three decades and has one of the most detailed long-term records of DOC concentration, water transparency, and PAR and UV light attenuation, in addition to other ecological data (Williamson et al. 2015; Knoll et al. 2018; Pilla et al. 2018). We assessed the improvement in model performance when including the new formulations, and systematically investigated the effects of long-term browning and increases in DOC on PAR and UV light attenuation, water temperature, and dissolved oxygen.

Methods:

Study site. Lake Giles is located in northeastern Pennsylvania, USA (41.377°N, 75.093°W; Fig. 1) on the Pocono Plateau at 428 m above sea level. Lake Giles has a catchment area of 1.83 km^2, lake surface area of 0.48 km^2, maximum depth of 24.1 m, volume of 4.88 x 10^6 m^3, and estimated retention time of 5.2 (Pilla et al. 2018) to 5.6 years (Moeller et al. 1995). The entire catchment of the lake is privately owned and well-protected, and the lake has one insubstantial ephemeral inflow stream and is otherwise spring water fed. Lake Giles was historically one of the clearest lakes in the northeastern USA, but has recently experienced strong effects of lake browning, with DOC concentrations more than doubling from 0.96 mg L^{-1} in 1993 to 2.48 mg L^{-1} in 2019 (Williamson et al. 2015, 2019). Concurrently, attenuation of PAR has increased from 0.12 m^{-1} to 0.34 m^{-1}, corresponding to 1% PAR penetration depths decreasing from 18.3 m to 13.0 m, respectively (Williamson et al. 2015, 2019). Similarly, attenuation of UV (320 nm) has increased from 0.41 m^{-1} to 2.81 m^{-1}, and corresponding 1% UV (320 nm) penetration depths of 9.7 m and 1.6 m, respectively (Williamson et al. 2015, 2019). The long-term physio-chemical consequences of increased DOC and decreased water transparency in lake Giles have been extensively studied as well. Pilla et al. (2018) reported significant surface water warming (1.04°C $decade^{-1}$), deepwater cooling (1.54°C $decade^{-1}$), increases in thermal stability (72.96 J m^{-2} $decade^{-1}$), and shallowing of thermocline depths (-1.00 m $decade^{-1}$) between 1988 and 2014. Knoll et al. (2018) found increased deepwater oxygen depletion and more prevalent anoxic conditions in Lake Giles during the same time period, associated with decreased water transparency and increased thermal stability. Biological responses of zooplankton taxa have also been preliminarily reported for Lake Giles, where decreases in crustacean grazers (*Daphnia* and calanoid copepods) and increases in a predatory, cold stenothermic cyclopoid copepod (*Cyclops scutifer*) have been observed (Williamson et al. 2015).

Meteorological data. Lake Giles does not have its own weather station. Instead, we relied on an on-lake weather station located 16.6 km away at Lake Lacawac for all the meteorological input data. Lake Lacawac is slightly smaller than Lake Giles (surface area of 0.21 km^2, maximum depth of 13.0 m), but is similarly well-protected with a fully forested shoreline. Meteorological data from this weather station has previously been used in conjunction with in-situ data for Lake Giles (Williamson et al. 2015; Pilla et al. 2018). Daily averages from 1997 through 2018 were used for the following meteorological variables (Supplementary Fig. S1): air temperature at 2 m (T_{air}; °C), global shortwave radiation (MJ m^{-2}), precipitation (mm day^{-1}), wind speed at 2 m (m sec^{-1}), relative humidity (%), and air pressure (hPa).

Inflow data. As there is only one minor, ephemeral inflow that is not monitored at Lake Giles, inflow volume was estimated based on total precipitation in the catchment and lake retention time. Daily inflow volume was estimated at 2,500 m^3 day^{-1} (0.03 m^3 s^{-1}) based on the volume and residence time of Lake Giles, resulting an approximate modelled residence time of 5.26 years. When air temperature was > 0°C, inflow was set to 2500 m^3 day^{-1}; when air temperature was ≤ 0°C, inflow volume was set to 0 m^3 day^{-1}, and accumulated for an inflow pulse on the next day when air temperature was > 0°C. Inflow temperature (T_{inflow}) was calculated as:

$$T_{inflow} = 5 + 0.75 \times T_{air} \quad (1)$$

per the methods of Stefan and Preud'homme (1993). Only one measurement of DOC in the inflow at Lake Giles has been recorded at 6.5 mg L^{-1} in summer 2003 (Cooke et al. 2006), so we used this as a guideline and estimated DOC in the inflow to mimic the long-term in-lake browning rates. We estimated DOC in the inflow as a constant 3 mg L^{-1} in the winter months of December through February. To force lake browning via the inflow, we set a baseline DOC value of 2.85 mg L^{-1} in the open-water months of March through November 1997, which then increased during the summer by 0.15 mg L^{-1} each year, resulting in a final inflow DOC concentration of 6 mg L^{-1} in 2018. Particulate organic carbon (POC) was set to 50% of the daily DOC in the inflow. Dissolved oxygen in the inflow was set to 100% saturation based on the daily air temperature and air pressure. All other chemical inflow variables were set to zero (Supplementary Fig. S2).

In-lake data. Long-term empirical data from Lake Giles from 1998 through 2018 was extracted from the data publication at the Environmental Data Initiative (Williamson 2019). Sampling methods and protocols follow general standards for limnological research. In brief, temperature and dissolved oxygen profiles were taken at 1 m increments with a Yellow Springs Instrument manual probe. Profiles of temperature were sparse from 1998 through 2006, and profiles of dissolved oxygen do not exist from 1998 through 2006. DOC samples were taken from discrete depth sampled at 0.5 m and 18 m, filtered through ashed 0.7 µm glass fiber filters, and analyzed through high temperature oxidation using a Shimadzu Total Organic Carbon Analyzer. PAR and UV light attenuation data, measured as $K_{d\ PAR}$ and $K_{d\ UV320}$, respectively, were calculated from a high-resolution vertical profiler using Biospherical Instruments Profiling UV radiometer or cosine compact four channel aquatic radiometer. For these manually collected data, samples generally occurred one to two times per month during the ice-free season.

High-frequency data of temperature and dissolved oxygen were collected with Precision Measurement Engineering miniDOT sensors sampling every 10 minutes from 2016 to 2018. All data were aggregated to the daily timestep by date and depth. Sensors were deployed from 16 October 2016 through 23 May 2018 at depths of 0.5 m and 22 m, and additional sensors were deployed starting 11 August 2017 through 23 May 2018 at depths of 4 m, 6 m, 8 m, 12 m, 14 m, 16 m, 18 m, 20 m, and 22 m. These high-frequency data sensors remained in the lake year-around, allowing for data collecting during the shoulder seasons and during ice cover, where manual sampling rarely occurs at Lake Giles. Sensor data from all depths were used for temperature data, and depths of 0.5 m and 22 m were using for dissolved oxygen data. Dissolved oxygen data at 22 m was removed from 06 April 2017 through 28 June 2017 due to sensor misplacement in the sediment where data were not reflective of water column processes. Despite the paucity of catchment data, the extensive long-term empirical data on the direct responses to lake browning (DOC, PAR and UV light attenuation) and ecological responses (thermal structure, dissolved oxygen, zooplankton abundance), combined with recent high-frequency sensor data on temperature and dissolved oxygen measured vertically in the water column consistently since October 2016, make Lake Giles a unique and highly suitable study lake to test model performance of lake browning scenarios.

Model selection & update. MyLake is an open-source, one-dimensional, processed-based model (Saloranta and Andersen 2007). It is a relatively concise MATLAB® code (MATLAB 2019) that has performed well with small boreal lakes experiencing browning and seasonal ice cover. Its recent iterations focused on dissolved oxygen (Couture et al. 2015), DOC (de Wit et al. 2018), CO_2 and CH_4 (Kiuru et al. 2019), and sediment-water interactions (Markelov et al. 2019). Here, we updated the publicly-available code described in Markelov et al. (2019), which estimated $K_{d\ PAR}$ solely based on changing chlorophyll concentration and not DOC concentration, with two additional parameters: β_{DOC} (Kiuru et al. 2019) and β'_{DOC}, which parametrize the time-varying response of PAR and UV light attenuation to DOC concentrations via calculations of $K_{d\ PAR}$ and $K_{d\ UV320}$, respectively.

$K_{d\ PAR}$ was previously calculated as:

$$K_{d\,PAR} = K_{d0} + \beta_{Chl} \times \overline{C}_z \qquad (2)$$

where K_{d0} is the attenuation value of PAR in pure distilled water (m^{-1}; Thrane et al. 2014), β_{Chl} is the optical cross-section or relative absorbance of chlorophyll (m^2 mg^{-1}), and $\overline{C}_z$ is the chlorophyll concentration at depth (mg m^{-3}). $K_{d\ PAR}$ now variably responds at each time step to DOC concentration in addition to chlorophyll concentration via the addition of the additional parameter β_{DOC}, which is the optical cross-section or PAR-specific relative absorbance of DOC in the water column (m^2 mg^{-1}). The resulting calculation of $K_{d\ PAR}$ in the new model update is:

$$K_{d\ PAR} = K_{d0} + \beta_{Chl} \times \overline{C}_z + \beta_{DOC} \times \overline{DOC}_z \qquad (3)$$

where $\overline{DOC}_z$ is DOC concentration at depth (mg m^{-3}; Kiuru et al, 2019). As $\overline{DOC}_z$ increases with lake browning, the resulting value of $K_{d\ PAR}$ calculated each time step will increase, indicating greater attenuation of PAR and reduced water transparency. The parameter β_{DOC} is analogous to the DOC absorbance, color, or chromophoric quality, and the relationship between $K_{d\ PAR}$ and $\overline{DOC}_z$ has been reported in several studies (Morris et al. 1995; Bukaveckas and Robbins-Forbes 2000; Read and Rose 2013; Thrane et al. 2014). These studies suggest that the β_{DOC} parameter value could theoretically be as low as zero, indicating no absorbance by DOC, or could range to as high as 0.725 m^2 mg^{-1} in a single lake (Morris et al. 1995). Across all the lakes included in these individual studies, estimates for β_{DOC} based on linear models ranged from 0.160 (n = 85, Bukaveckas and Robbins-Forbes 2000), 0.217 (n = 7, Read and Rose 2013), to 0.222 (n = 65, Morris et al. 1995). The low DOC-specific absorbance empirical measurements in Lake Giles that are analogous to the β_{DOC} parameter suggest that β_{DOC} may be lower in Lake Giles than these across-lake estimates (Williamson et al. 2015; Pilla et al. 2018).

The model also calculates a new state variable, $K_{d\ UV320}$, based on its linear relationship with $\overline{DOC}_z$ from the equation:

$$K_{d\ UV320} = K'_{d0} + \beta'_{DOC} \times \overline{DOC}_z \qquad (4)$$

where K'_{d0} and β'_{DOC} represent the same theoretical parameters as for $K_{d\ PAR}$, but relative to UV attenuation and absorption. Since DOC selectively absorbs UV wavelengths relative to PAR wavelengths (Williamson et al. 1996), these parameter values are not expected to be equivalent to those used for calculating light attenuation of PAR and are thus calibrated independently. Further details on this model description and relevant parameters can be found in the Supplemental Material and Supplemental Table S1.

Model calibration. Model calibration spanned the period of in-lake data from 16 October 2016 through 23 May 2018 and included five state variables: DOC, $K_{d\ PAR}$, $K_{d\ UV320}$, water temperature, and dissolved oxygen. This period was selected as it allows testing the model against both manually-sampled data of these five state variables as well as high-frequency sensor data of temperature and dissolved oxygen data as described above. Twenty-three parameters were included in model calibration (Supplemental Table S1). The diagnostic index was RMSE-observations standard deviation ratio (RSR; Moriasi et al. 2007) for each state variable across all included depths, then summed across the five state variables, as follows:

$$\Sigma RSR = \sum_{i=1}^{n} \frac{RMSE}{\sigma_{obs}} \qquad (5)$$

RSR is a useful diagnostic index when calibrating across multiple state variables with different units, as it includes a scaling or normalizing factor. An RSR value ≤ 0.70 suggests satisfactory model performance (Moriasi et al. 2007). The Nelder-Mead simplex optimization routine (Box 1965; Nelder and Mead 1965) was used to minimize the diagnostic index ΣRSR using the "nloptr" package in R (Johnson 2018).

Model scenarios of seasonal DOC fluctuation and light attenuation responses. We created two artificial scenarios with short-term, seasonal fluctuations in DOC concentration in the inflows for a one year simulation to test the response of in-lake DOC, $K_{d\ PAR}$, and $K_{d\ UV320}$ in the updated model (Fig. 2). Scenario A increased inflow DOC concentration on a monthly basis from no DOC in January and by 2 mg L^{-1} from February through May up through an inflow concentration of 10 mg L^{-1} maintained in June and July. Inflow DOC concentration was then decreased on a monthly basis by 2 mg L^{-1} from August until December, when it again returned to zero. Scenario B assessed rapid fluctuations in inflow DOC concentration that reverted between zero and 6 mg L^{-1} every other month from January through December. For both scenarios, we assessed the short-term responses of in-lake DOC, $K_{d\ PAR}$, and $K_{d\ UV320}$ that were not as easily captured in the 20-year simulation due to limited empirical inflow data.

Model backcast in Lake Giles. We used a backcast scenario initialized with in-situ profiles from Giles on 05 August 1997 with the described meteorological and inflow conditions, and reported output beginning 01 January 1998 after a 5-month model spin-up. We ran a 20-year simulation in Giles through 31 December 2018 using either the fixed K_d version or the varying $K_{d\ PAR}$ and $K_{d\ UV320}$ version. Long-term trends for empirical data and model outputs were assessed with Mann-Kendall non-parametric trend tests with Sen's slopes using the "trend" package in R (Pohlert 2018) using $\alpha = 0.05$.

All analyses were completed in R version 3.6.2 (R Core Team 2019), using the "R.matlab" package (Bengtsson 2018) for communication with and execution of MyLake MATLAB scripts (MATLAB 2019). All figures were created using the "ggplot2" (Wickham 2016) and "ggpubr" packages in R (Kassambara 2019).

Results:

Model calibration & evaluation. Calibration of the updated model version against five state variables at multiple depths resulted overall in satisfactory model agreement with observed data (Table 1, Supplemental Fig. S3). Calibration performance for key state variable ranked best for temperature, then dissolved oxygen, $K_{d\ UV320}$, $K_{d\ PAR}$, and finally worst for DOC. Versus depth, model performance for temperature and dissolved oxygen was best at the surface, consistent with the boundary conditions of one-dimensional models being at the air-water interface for these two state variables. In contrast, performance for DOC was better at the bottom of the water column, consistent with their boundary conditions being at the inflow. This is the first time that DOC at multiple depths has been used in a calibration routine, alongside high-frequency water temperature and dissolved oxygen data, leaving room for improvement especially in systems where inflow data are readily monitored.

There were two notable limitations during the calibration period. For DOC, $K_{d\ PAR}$, and $K_{d\ UV320}$ the model tended toward an average rather than highlighting the seasonal variability found in the 2-year calibration period (Supplemental Fig. S4, Fig. S5). However, there were few in-lake measurements for these variables during the calibration period (n = 11), and the manually-derived increased DOC concentrations in the inflow under-represents natural short-term variations in DOC and the consequent responses in $K_{d\ PAR}$ or $K_{d\ UV320}$. Second, the was a discrepancy during the ice-cover period during March 2018 for water temperature and dissolved oxygen (Supplemental Fig. S6, Fig. S7), where the model suggested an extended period of ice cover that was not observed at the lake. We elected to remove the data from 01 March 2018 through 31 March 2018 from the calibration so that the error in ice-off prediction did not skew the model calibration for temperature or other state variables. Overall, all state variables at all depths were deemed satisfactorily calibrated in the updated model version of MyLake to be used for further modelling scenarios (Supplemental Fig. S3).

Seasonal DOC fluctuation scenarios. In both Scenario A and Scenario B, all three in-lake measures of water transparency responded rapidly to the changing fluxes of inflow DOC concentration (Fig. 2). During winter, responses were more variable due to the delayed inflow volume resulting from the assumption of frozen surface water. However, in the open-water season, in-lake DOC (Fig. 2c, 2d), $K_{d\ PAR}$ (Fig. 2e, 2f), and $K_{d\ UV320}$ (Fig. 2g, 2h) responded rapidly to these artificial scenarios with the expected direction and magnitude of change. Also as expected, responses in $K_{d\ UV320}$ were an order of magnitude greater than that of $K_{d\ PAR}$ due to the greater selective absorption of shorter wavelengths by DOC. Hence, we found this model update to have adequate short-term responsiveness for the key in-lake water transparency variables to changing inflow DOC concentrations.

Backcast model validation in Lake Giles. Both the varying K_d and fixed K_d models showed satisfactory model performance of DOC concentration in the 1998-2018 backcast scenario that mimicked long-term lake browning (Table 2, Fig. 3a, 3b). For DOC, the two model versions were essentially indistinguishable because the inflow of DOC was equivalent for both estimates of in-lake DOC. DOC significantly increased during summer at a rate of 0.050 mg L^{-1} $year^{-1}$ in both models ($p < 0.001$ for both), only slightly slower than the increase in the observed data of 0.070 mg L^{-1} $year^{-1}$ ($p < 0.001$, Table 3).

In contrast, only the varying K_d model reproduced the observed long-term responses of $K_{d\ PAR}$ (Fig. 3c, 3d) and $K_{d\ UV320}$ (Fig. 3e, 3f) to increases in DOC concentration (Table 3). The varying K_d model had significantly increasing $K_{d\ PAR}$ at a rate of 0.006 m^{-1} $year^{-1}$ ($p < 0.001$), comparable to the observed rate of increase of 0.009 m^{-1} $year^{-1}$ ($p < 0.001$), while the fixed K_d model showed no change in $K_{d\ PAR}$ (Table 3). Similarly, $K_{d\ UV320}$ from the varying K_d model increased at a rate of 0.052 m^{-1} $year^{-1}$ ($p < 0.001$) compared to the observed rate of increase of 0.090 m^{-1} $year^{-1}$ ($p < 0.001$), and showed no change in the fixed K_d model (Table 3).

In both the fixed and varying K_d models, surface water temperature performed very well (Table 2, Fig. 4a, 4b). However, the rates of surface water warming compared to the observed trend of 0.120°C $year^{-1}$ ($p = 0.15$) was better modelled in the varying K_d model, with a warming rate of 0.093°C $year^{-1}$ ($p = 0.07$), versus the fixed K_d model rate of 0.051°C $year^{-1}$ ($p = 0.22$; Table 3). The main difference between fixed and varying K_d models was observed cooling of deep waters at a rate of -0.072°C $year^{-1}$ ($p = 0.08$), which was only simulated using the varying K_d model (Table 2, Fig. 4c, 4d). In the varying K_d model, deepwater temperature decreased significantly at a rate of -0.097°C $year^{-1}$ ($p < 0.001$), compared to no change in the fixed K_d model ($p = 0.53$; Table 3).

Similar to surface water temperature, simulated surface dissolved oxygen performed equally well for both the fixed and varying K_d models (Table 2, Fig. 5a, 5b). While there was no significant observed change in surface dissolved oxygen (-0.016 mg L^{-1} $year^{-1}$, $p = 0.30$), the varying K_d model resulted in a significant decrease in surface dissolved oxygen at a rate of -0.017 mg L^{-1} $year^{-1}$ ($p = 0.04$) compared to no significant change in the fixed K_d model (-0.008 mg L^{-1} $year^{-1}$, $p = 0.24$). Finally, deepwater dissolved oxygen had better model performance in the varying K_d model (Table 3, Fig. 5c, 5d), showing greater deepwater oxygen depletion (-0.118 mg L^{-1} $year^{-1}$, $p = 0.06$) compared to no significant change in the fixed K_d model (-0.022 mg L^{-1} $year^{-1}$, $p = 0.53$). Though the observed data here only span 2007 to 2018 with no significant trend over this time period (Table 3), Knoll et al. (2018) reported long-term decreases from 1988 to

2014 at a rate of -0.163 mg L^{-1} $year^{-1}$, much more comparable to the simulated decrease in deepwater dissolved oxygen in the varying K_d model.

Discussion:

The new model update presented here successfully replicates short-term in-lake DOC dynamics and the expected PAR and UV attenuation responses, as well as long-term browning patterns and structural vertical changes in a model lake ecosystem, Lake Giles. The varying K_d model improved estimates over 20 years by up to 52% across five state variables, and especially improved long-term trends in deepwater variables, which are particularly sensitive to increased light attenuation and thermal stability (Knoll et al. 2018; Pilla et al. 2018). Though the important connections between DOC and light attenuation have long been established (Morris et al. 1995; Williamson et al. 1996; Pace and Cole 2002), this is the first lake model to incorporate varying light attenuation that is responsive to daily changes in DOC concentration. Further, we developed the first modelling of UV attenuation that is also variably responsive to DOC concentration, and which is a key response to browning with important implications for photobleaching feedbacks (Cory et al. 2014) and trophic interactions (Williamson et al. 2015). This model that can successfully reproduce short- and long-term ecosystem responses to DOC fluctuations and lake browning, an important feature for future studies aiming to improve understanding of the drivers and responses of DOC fluxes in lakes, including feedback loops, biological responses, and water quality (Solomon et al. 2015; Williamson et al. 2015).

This model has the capability to assess rapid, short-term changes in DOC concentration and responses of light attenuation. Short-term fluctuations in DOC due to storm and precipitation events are common (Zhang et al. 2010; de Wit et al. 2016; Rose et al. 2017), and can reduce

PAR and UV transparency in lakes by over 7% in one day (Williamson et al. 2016), with important influences on resultant structural and biological responses. For example, rapid reductions in PAR and UV penetration following an intense summer storm led to an upward shift in the vertical distribution of zooplankton in Lake Lacawac (Pennsylvania, USA), with potential implications for changes in predator-prey overlap (Rose et al. 2012). Similarly, rapid reductions in underwater UV irradiance in one day by just 9% due to short-term smoke plumes at Lake Tahoe (California, USA) resulted in 4.1 m shallower vertical distribution of zooplankton, but with no change in the vertical distribution of their predators (Urmy et al. 2016). In the Lake Giles long-term backcast, we were not able to capture these shorter-term seasonal patterns in DOC and light attenuation, even in the varying K_d model. This is likely due to the manually-estimated inflow volume and DOC concentration that limited the seasonal or episodic fluctuations of in-lake DOC and therefore of $K_{d\ PAR}$ and $K_{d\ UV320}$ during storm events or seasonal precipitation patterns. We expect that systems with detailed empirical inflow volume and DOC concentration data would be useful case studies to understand associated in-lake responses to patterns in DOC at different temporal scales, and to further improve the model's performance.

The inclusion of UV attenuation in this model as a time-varying variable to changing DOC is, to our knowledge, the first of its kind. While estimates for $K_{d\ UV320}$ in Lake Giles would be possible based on published empirical relationships between $K_{d\ UV320}$ and DOC concentrations across lakes, as in Morris et al. (1995), we found this led to a two-fold overestimation of $K_{d\ UV320}$ values, and therefore would result in inaccurate predictions for chemical and ecological consequences of browning. This overestimation for $K_{d\ UV320}$ was likely due to the distinctively low DOC absorption coefficient of UV wavelengths of Lake Giles's water, in which it falls in the 3rd percentile of lowest DOC absorption values (Morris et al. 1995). Though there is a strong empirical relationship between DOC concentration and $K_{d\ UV320}$ as presented in in Morris et al. (1995), an estimation of $K_{d\ UV320}$ exclusively from DOC concentration ignores the role that very low DOC absorption values also contribute to estimations of $K_{d\ UV320}$. The lake-specific calibration enhanced the model performance for predicting $K_{d\ UV320}$ by 52% compared to a fixed, low value of the UV-specific DOC absorption parameter, β'_{DOC} (Supplemental Table S1). Hence, the calibration of DOC absorption as the β'_{DOC} parameter in addition to varying DOC concentration in our model update's estimation of $K_{d\ UV320}$ was the key reason we saw such notable improvement in $K_{d\ UV320}$.

Nevertheless, the impact of DOC on light attenuation remains more dynamic than what is included in this model update. In particular, DOC absorption coefficients have been increasing in Lake Giles alongside DOC concentration (Williamson et al. 2015), and in most recent years has increased by more than six-fold of the original value presented in Morris et al. (1995; Williamson et al. 2019). While the β_{DOC} and β'_{DOC} parameters were calibrated to Lake Giles, their values were fixed and did not change over time, which suggests the model may still be lacking finer precision of both $K_{d\ PAR}$ and $K_{d\ UV320}$ estimates. Hence, time series data of wavelength-specific DOC absorption, in addition to DOC concentration, would allow implementing β_{DOC} and β'_{DOC} as state variables rather than parameters and further improve modelling of decreasing $K_{d\ PAR}$ and $K_{d\ UV320}$ due to browning. In particular, photobleaching rates, which depends heavily on surface light attenuation, remain a poorly constrained DOC sink, especially in northern waters (Ward and Cory 2020; De Wit et al. 2018).

The ecosystem variables of interest in the browning scenario at Lake Giles resulted in the expected rapid increases in PAR and UV light attenuation, warming surface waters, cooling deep waters, and decreasing deepwater dissolved oxygen. These quintessential responses to long-term browning are a result of the greater absorption of light and heat in the surface waters with higher DOC concentrations and thereby higher $K_{d\ PAR}$, leading to strong changes in vertical heat penetration that reduce deepwater temperatures (Read and Rose 2013; Rose et al. 2016; Pilla et al. 2018), which were not captured when using the fixed K_d model. These thermal patterns occurred here in the absence of air temperature warming at Lake Giles due to the increased heat trapping capabilities of colored DOC in the surface waters (Pilla et al. 2018; Supplemental Fig. S1a), which has also been observed in other lakes (Rose et al. 2016; Bartosiewicz et al. 2019). This diverging response of surface vs. deep waters to browning has been previously reported in Lake Giles (Williamson et al. 2015; Pilla et al. 2018) and in other lakes as a "shielding" of deep waters due to greater light and heat absorption in the surface waters (Bartosiewicz et al. 2019). We suggest that this diverging pattern and resultant increase in thermal stability (Pilla et al. 2018) drove the decreasing deepwater dissolved oxygen concentrations. Because our modelling scenarios had equivalent increases in in-lake DOC and thereby carbon substrate, increased microbial decomposition was not a reasonable mechanism for the decreases in dissolved oxygen, as has been proposed in other studies (Couture et al. 2015). We would expect similar responses in thermal structure and deepwater dissolved oxygen primarily in lakes with low DOC concentrations and low K_d values, as these clear lakes tend to be much more sensitive than less transparent lakes to inputs of DOC concentration and changes in light attenuation (Snucins and Gunn 2000; Rose et al. 2016) due to the exponential relationship between light penetration and DOC concentration (Williamson et al. 1996). Empirical studies of nearby Lake Lacawac, which is experiencing similar patterns of long-term browning but had initially-higher DOC concentrations, have shown much more muted changes in light attenuation, thermal structure, and oxygen depletion compared to Lake Giles (Williamson et al. 2015; Knoll et al. 2018; Pilla et al. 2018). Further study of the mechanisms driving these key structural responses over a range of lake transparencies, with modelling scenarios such as those in Fig. 2, can pinpoint the most sensitive types of lakes and response variables, especially as global changes in thermal structure (Pilla et al. 2020) and deepwater oxygen depletion (Jenny et al. 2016) become more prevalent.

The modelling work here highlights a number of feedback loops related to the estimation of $K_{d\ PAR}$ and $K_{d\ UV320}$ when DOC concentrations vary. For example, photo-processing by UV light alters both the color and concentration of DOC (Zhang et al. 2010; Cory et al. 2014), and these changes in DOC would therefore feed back into the estimation of both $K_{d\ PAR}$ and $K_{d\ UV320}$. In fact, photo-processing is often more important than biodegradation of carbon (Dempsey et al. 2020) and can account for up to 95% of total carbon processing in Arctic systems (Cory et al. 2014). In Lake Giles, photo-processing resulted in nearly a 50% decrease in DOC absorption coefficients in just one week (Dempsey et al. 2020), again highlighting the importance of incorporation of DOC absorption or color in addition to DOC concentration for estimating light attenuation. Further, in lakes experiencing diverging surface vs. deepwater temperature patterns and consequent increases in thermal stability, residence time of water and DOC tends to increase, which is an important control of DOC processing in lakes (Cory et al. 2015; Catalán et al. 2016). Conversely, increases in precipitation events that tend to be associated with long-term lake browning shorten residence time and flush DOC out of lakes, limiting time for photo-processing (de Wit et al. 2018). Hence, the interaction between photo-processing and residence time (Cory et al. 2015) and their influence on DOC concentration, color, and reactivity are key considerations for modelling applications and advances. These feedback loops between DOC and both $K_{d\ PAR}$ and $K_{d\ UV320}$ will also, in turn, control vertical thermal structure and oxygen depletion especially in high transparency lakes like Lake Giles due to their greater sensitivity compared to low transparency systems (Snucins and Gunn 2000; Read and Rose 2013; Rose et al. 2016; Pilla et al. 2018).

In conclusion, incorporating dynamic linkages between DOC and light attenuation at multiple wavelengths in lake ecosystem models is essential for accurate modelling applications of lake browning, including vertical structural responses to changing light attenuation, oxygen depletion rates, and effects on photo-processing feedback loops. Further model advancements include implementing varying DOC absorption to understand the suite of ecological consequences and potential feedback loops related to photo-processing and residence time in browning lakes. As the ramifications of long-term lake browning are not currently well understood (Solomon et al. 2015), innovative modelling studies of lake browning that develop and implement optical responses across multiple biologically-relevant light wavelengths can provide a unique understanding of the potential changes in lake ecosystems due to increased DOC concentration and color, ranging from microbial processing to trophic interactions to greenhouse gas emissions.

References:

Bartosiewicz, M., A. Prsytulska, J.-F. Lapierre, I. Laurion, M. D. Lehmann, and R. Maranger. 2019. Hot tops, cold bottoms: Synergistic climate warming and shielding effects increase carbon burial in lakes. Limnol. Oceanogr. Lett. doi:10.1002/lol2.10117

Bengtsson, H. 2018. R.matlab: Read and write MAT files and call MATLAB from within R.

Box, M. J. 1965. A New Method of Constrained Optimization and a Comparison with Other Methods. The Computer Journal 8: 42-52.

Brothers, S., J. Köhler, K. Attermeyer, H. P. Grossart, T. Mehner, N. Meyer, K. Scharnweber, and S. Hilt. 2014. A feedback loop links brownification and anoxia in a temperate, shallow lake. Limnol. Oceanogr. 59: 1388-1398.

Bukaveckas, P. A. and M. Robbins-Forbes. 2000. Role of dissolved organic carbon in the attenuation of photosynthetically active and ultraviolet radiation in Adirondack lakes. Freshwater Biol. 43: 339-354.

Catalán, N., R. Marcé, D. N. Kothawala, and L. J. Tranvik. 2016. Organic carbon decomposition rates controlled by water retention time across inland waters. Nat. Geosci. doi:10.1038/NGEO2720

Cooke, M. S., M. D. Evans, M. Dizdaroglu, and J. Lunec. 2003. Oxidative DNA damage: mechanisms, mutation, and disease. FASEB J. 17: 1195-1214.

Cooke, S. L., C. E. Williamson, B. R. Hargreaves, and D. P. Morris. 2006. Beneficial and detrimental interactive effects of dissolved organic matter and ultraviolet radiation on zooplankton in a transparent lake. Hydrobiologia 568: 15-28.

Cory, R. M., C. P. Ward, B. C. Crump, and G. W. Kling. 2014. Sunlight controls water column processing of carbon in arctic fresh waters. Science 345: doi:10.1126/science.1253119

Cory, R. M., K. H. Harrold, B. T. Neilson, and G. W. Kling. 2015. Controls on dissolved organic matter (DOM) degradation in a headwater stream: the influence of photochemical and hydrological conditions in determining light-limitation or substrate-limitation of photo-degradation. Biogeosciences 12: 6669-6685.

Couture, R.-M., H. A. de Wit, K. Tominaga, P. Kiuru, and I. Markelov. 2015. Oxygen dynamics in a boreal lake responds to long-term changes in climate, ice phenology, and DOC inputs. J. Geophys. Res.: Biogeosci. 120: doi:10.1002/2015JG003065

de Wit, H. A., R.-M. Couture, L. Jackson-Blake, M. N. Futter, K. Austnes, J.-L. Guerrero, and Y.

Lin. 2018. Pipe or chimneys? For carbon cycling in small boreal lakes, precipitation matters most. Limnol. Oceanogr. Lett. doi:10.1002/lol2.10077

Dempsey, C. M. and others. 2020. The relative importance of photodegradation and biodegradation of terrestrially derived dissolved organic carbon across four lakes of differing trophic status. Biogeosciences doi:10.5194/bg-2020-160

de Wit, H. A., and others. 2016. Current Browning of Surface Waters Will Be Further Promoted by Wetter Climate. Environ. Sci. Technol. Lett. 3: 430-435.

Evans, C. D., P. J. Chapman, J. M. Clark, D. T. Monteith, and M. S. Cressers. 2006. Alternative explanations for rising dissolved organic carbon export from organic soils. Global Change Biology 12: doi:10.1111/j.1365-2486.2006.01241.x

Hansen, G. J. A., L. A. Winslow, J. R. Read, M. Treml, P. J. Schmalz, and S. R. Carpenter. 2019. Water clarity and temperature effects on walleye safe harvest: an empirical test of the safe operating space concept. Ecosphere 10: doi:e02737. 10.1002/ecs2.2737

Jenny, J.-P., P. Francus, A. Normandeau, F. Lapointe, M.-E. Perga, A. Ojala, A. Schimmelmann, and B. Zolitschka. 2016. Global spread of hypoxia in freshwater ecosystems during the last three centuries is caused by rising local human pressure. Global Change Biology 22: 1481-1489.

Johnson, S. G. 2018. The NLopt non-linear optimization package.

Kassambara, A. 2019. ggpubr: "ggplot2" based publication ready plots.

Kiuru, P., A. Ojala, I. Mammarella, J. Heiskanen, K.-M. Erkkilä, H. Miettinen, T. Vesala, and T. Huttula. 2019. Applicability and consequences of the integration of alternative models for CO2 transfer velocity into a process-based lake model. Biogeosciences 16: 3297-3317.

Knoll, L. B., C. E. Williamson, R. M. Pilla, T. H. Leach, J. A. Brentrup, and T. J. Fisher. 2018.

Browning-related oxygen depletion in an oligotrophic lake. Inland Waters doi:10.1080/20442041.2018.1452355

Markelov, I., R.-M. Couture, R. Fischer, S. Haane, and P. Van Cappellen. 2019. Coupling Water Column and Sediment Biogeochemical Dynamics: Modeling Internal Phosphorus Loading, Climate Change Responses, and Mitigation Measures in Lake Vansjø, Norway. J. Geophys. Res.: Biogeosci. 124: doi:10.1029/2019JG005254

MATLAB. (2019). version 9.6.0.1072779 (R2019a). Natick, Massachusetts: The MathWorks Inc.

Moeller, R. E., C. E. Williamson, B. R. Hargreaves, and D. P. Morris. 1995. Limnology of Lakes Lacawac, Giles, and Waynewood 1989-1993: An introduction to the core lakes of the Pocono Comparative Lakes Program. Available from Lehigh University Library by Interlibrary Loan System, Bethlehem, PA, USA.

Monteith, D. T., and others. 2007. Dissolved organic carbon trends resulting from changes in atmospheric deposition chemistry. Nature 450: doi:10.1038/nature06316

Moriasi, D. N., J. G. Arnold, M. W. Van Liew, R. L. Bingner, R. D. Harmel, and T. L. Veith. 2007. Model Evaluation Guidelines for Systematic Quantification of Accuracy in Watershed Simulations. Trans. ASABE 50: 885-900.

Morris, D. P., H. Zagarese, C. E. Williamson, E. G. Balseiro, B. R. Hargreaves, B. Modenutti, R. Moeller, and C. Queimalinos. 1995. The attenuation of solar UV radiation in lakes and the role of dissolved organic carbon. Limnol. Oceanogr. 40: 1381-1391.

Nelder, J. A. and R. Mead. 1965. A simplex method for function minimization. The Computer Journal 7: 308-313.

Overholt, E. P., S. R. Hall, C. E. Williamson, C. K. Meikle, M. A. Duffy, and C. E. Cáceres.

2012. Solar radiation decreases parasitism in *Daphnia*. Ecology Letters 15: 47-54.

Pace, M. I. and J. J. Cole. 2002. Synchronous Variation of Dissolved Organic Carbon and Color in Lakes. Limnol. Oceanogr. 47: 333-342.

Paerl, H. W. and T. G. Otten. 2013. Blooms Bite the Hand That Feeds Them. Science 342: 433-434.

Pilla, R. M., C. E. Williamson, J. Zhang, R. L. Smyth, J. D. Lenters, J. A. Brentrup, L. B. Knoll, and T. J. Fisher. 2018. Browning-Related Decreases in Water Transparency Lead to Long-Term Increases in Surface Water Temperature and Thermal Stratification in Two Small Lakes. J. Geophys. Res.: Biogeosci. 123: doi:10.1029/2017JG004321

Pilla, R. M. and others. 2020. Deeper waters are changing less consistently than surface waters in a global analysis of 102 lakes. Sci. Rep. doi:10.1038/s41598-020-76873-x

Pohlert, T. 2018. trend: Non-parametric trend tests and change-point detection.

R Core Team. 2019. R: A language and environment for statistical computing. R Foundation for Statistical Computing. Vienna, Austria.

Read, J. S. and K. C. Rose. 2013. Physical responses of small temperate lakes to variation in dissolved organic carbon concentrations. Limnol. Oceanogr. 58: 921-931.

Rose, K. C., C. E. Williamson, J. M. Fischer, S. J. Connelly, M. Olson, A. J. Tucker, and D. A. Noe. 2012. The role of ultraviolet radiation and fish in regulating the vertical distribution of *Daphnia*. Limnol. Oceanogr. 57: 1867-1876.

Rose, K. C., L. A. Winslow, J. S. Read, and G. J. A. Hansen. 2016. Climate-induced warming of lakes can be either amplified or suppressed by trends in water clarity. Limnol. Oceanogr. Lett. doi:10.1002/lol2.10027

Rose, K. C., S. R. Greb, M. Diebel, and M. G. Turner. 2017. Annual precipitation regulates spatial and temporal drivers of lake water clarity. Ecological Applications 27: 632-643.

Roulet, N. and T. R. Moore. 2006. Browning the waters. Nature 444: 283-284.

Saloranta, T. M. and T. Andersen. 2007. MyLake—A multi-year lake simulation model code suitable for uncertainty and sensitivity analysis simulations. Ecol. Modell. 207: 45-60.

Snucins, E. and J. Gunn. 2000. Interannual variation in the thermal structure of clear and colored lakes. Limnol. Oceanogr. 45: 1639-1646.

Solomon, C. T., and others. 2015. Ecosystem Consequences of Changing Inputs of Terrestrial Dissolved Organic Matter to Lakes: Current Knowledge and Future Challenges. Ecosystems 18: 376-389.

Stefan, H. G. and E. B. Preud'homme. 1993. Stream temperature estimation from air temperature. Water Resour. Bull. 29: 27-45.

Strock, K. E., S. J. Nelson, J. S. Kahl, J. E. Saros, and W. H. McDowell. 2014. Decadal Trends Reveal Recent Acceleration in the Rate of Recovery from Acidification in the Northeastern U.S. Environ. Sci. Technol. doi:10.1021/es404772n

Thrane, J.-E., D. O. Hessen, and T. Andersen. 2014. The absorption of light in lakes: Negative impact of dissolved organic carbon on primary productivity. Ecosystems 14: 1040-1052.

Urmy, S. S., C. E. Williamson, T. H. Leach, S. G. Schladow, E. P. Overholt, and J. D. Warren. 2016. Vertical redistribution of zooplankton in an oligotrophic lake associated with reduction in ultraviolet radiation by wildfire smoke. Geophys. Res. Lett. 43: 3746-3753.

Ward, C. P. and R. M. Cory. 2020. Assessing the prevalence, products, and pathways of dissolved organic matter partial photo-oxidation in arctic surface waters. Environ. Sci.: Processes Impacts 22: 1214-1223.

Wauthy, M., M. Rautio, K. S. Christoffersen, L. Forsström, I. Laurion, H. L. Mariash, S. Peura, and W. F. Vincent. 2018. Increasing dominance of terrigenous organic matter in circumpolar freshwaters due to permafrost thaw. Limnol. Oceanogr. Lett. 3: 186-198.

Wickham, H. 2016. ggplot2: Elegant graphics for data analysis. Springer-Verlag, New York.

Williamson, C. E., R. S. Stemberger, D. P. Morris, T. M. Frost, and S. G. Paulson. 1996. Ultraviolet radiation in North American lakes: Attenuation estimates from DOC measurements and implications for plankton communities. Limnol. Oceanogr. 41: 1024-1034.

Williamson, C. E., B. R. Hargreaves, P. S. Orr, and P. A. Lovera. 1999. Does UV play a role in changes in predation and zooplankton community structure in acidified lakes? Limnol. Oceanogr. 44: 774-783.

Williamson, C. E., E. P. Overholt, R. M. Pilla, T. H. Leach, J. A. Brentrup, L. B. Knoll, E. M. Mette, and R. E. Moeller. 2015. Ecological consequences of long-term lake browning. Sci. Rep. 5: doi:10.1038/srep18666

Williamson, C. E., and others. 2016. Sentinel responses to droughts, wildfires, and floods: effects of UV radiation on lakes and their ecosystem services. Front. Ecol. Environ. 14: doi:10.1002/fee.1228

Williamson, C. E., and others. 2017. Climate change-induced increases in precipitation are reducing the potential for solar ultraviolet radiation to inactivate pathogens in surface waters. Sci. Rep. 7: doi:10.1038/s41598-017-13392-2

Williamson, C. E. 2019. Three decades of limnological data from lakes in the Pocono Mountains region, Pennsylvania, USA, 1988-2018, version 1. Environmental Data Initiative. doi.org/10.6073/pasta/834c813f123c8faf3d59477e54bfc3ce

Wolf, R., T. Andersen, D. O. Hessen, and K. Hylland. 2017. The influence of dissolved organic carbon and ultraviolet radiation on the genomic integrity of *Daphnia magna*. Functional Ecology 31: 848-855.

Wolf, R., J.-E. Thrane, D. O. Hessen, and T. Andersen. 2018. Modelling ROS formation in boreal lakes from interactions between dissolved organic matter and absorbed solar photon flux. Water Research 132: 331-339.

Zhang, J., and others. 2010. Long-term patterns of dissolved organic carbon in lakes across eastern Canada: Evidence of a pronounced climate effect. Limnol. Oceanogr. 55: 30-42.

Acknowledgements:

RMP was supported by the Sentinel North Research Internship Scholarship program for foreign students at Université Laval, and by NSF DEB 1950170, 1754276, and 1754265 grants. This research was also supported the Sentinel North program of Université Laval, made possible, in part, thanks to funding from the Canada First Research Excellence Fund. RMC acknowledges funding from the NSERC Discovery grant program. Data collection at Lake Giles was supported by Craig Williamson's Global Change Limnology Laboratory at Miami University and E. P. Overholt, and Kevin Rose's Global Water Laboratory at Rensselaer Polytechnic Institute. We thank Lacawac Sanctuary and Biological Field Station and B. R. Hargreaves for collection of and access to meteorological data. Model code and data from this application are available at https://github.com/biogeochemistry. The authors declare no conflicts of interest.

Tables:

Table 1. Diagnostic model performance statistics for the calibration period. Diagnostic indices include root mean squared error (RMSE), bias, RMSE-observations standard deviation ratio (RSR), and mean absolute percentage error (MAPE).

Variable	Depth (m)	RMSE	Bias	RSR	MAPE (%)
DOC	0.5	0.145	-0.012	1.076	5.0
	18	0.183	-0.011	0.851	8.5
$K_{d\ PAR}$	0.5	0.045	-0.001	0.930	12.8
$K_{d\ UV320}$	0.5	0.357	0.002	0.855	12.1
Water Temperature	4	1.200	0.116	0.163	19.9
	6	1.031	-0.136	0.147	18.3
	8	1.763	-0.853	0.345	21.0
	12	1.321	-0.696	0.669	21.9
	14	1.032	-0.522	0.737	19.9
	16	0.818	-0.330	0.717	16.9
	18	0.714	-0.221	0.703	14.8
	20	0.645	-0.116	0.694	12.2
	22	0.583	-0.011	0.691	10.7
Dissolved Oxygen	0.5	0.776	-0.095	0.510	5.7
	22	1.591	-0.014	0.338	866.0

Table 2. Diagnostic model performance statistics for the validation period under both the fixed K_d and varying K_d model versions. Diagnostic indices include root mean squared error (RMSE), bias, RMSE-observations standard deviation ratio (RSR), and mean absolute percentage error (MAPE).

Variable	Depth (m)	RMSE		Bias		RSR		MAPE (%)	
		fixed	varying	fixed	varying	fixed	varying	fixed	varying
DOC	0.5	0.264	0.264	0.062	0.007	0.523	0.522	11.5	12.5
$K_{d\ PAR}$	0.5	0.104	0.094	-0.036	0.038	1.066	0.967	35.5	19.5
$K_{d\ UV320}$	0.5	0.936	0.516	-0.634	0.106	1.356	0.748	77.6	26.0
Water Temperature	2	0.910	0.895	-0.226	0.447	0.182	0.179	4.1	4.1
	20	1.460	0.628	1.318	0.265	2.173	0.935	22.7	8.0
Dissolved Oxygen	2	0.838	0.867	-0.216	-0.312	0.618	0.639	6.6	7.3
	20	3.138	2.816	1.905	0.881	0.972	0.872	103.2	159.2

Table 3. Comparison of Sen's slope estimated trends from summer averages spanning 1998-2018 between observed data, fixed K_d model, and varying K_d model. Asterisks indicate statistically significant trends ($p < 0.05$).

Variable	Depth	Sen's Slope ($year^{-1}$)		
		observed	**fixed**	**varying**
DOC	surface	0.070*	0.050*	0.050*
$K_{d\ PAR}$	surface	0.009*	0.000	0.006*
$K_{d\ UV320}$	surface	0.090*	0.000	0.052*
Water Temperature	surface	0.120	0.051	0.093
	deepwater	-0.072	0.002	-0.097*
Dissolved Oxygen	surface	-0.016	-0.008	-0.017*
	deepwater	0.023	-0.022	-0.118

Figure Legends:

Figure 1. (a) Location of Lake Giles in northeastern Pennsylvania (blue point), and (b) bathymetric map of Lake Giles. Blue point in the center of the lake indicates the sampling location of manual samples and profiles and the mooring station of high-frequency sensors. Brown triangle in the lake shore indicates the approximate location of the ephemeral inflow stream.

Figure 2. Scenarios A and B testing responsiveness to seasonal fluctuations of artificial time-series (black dashed lines) of (a, b) inflow DOC concentration, and the corresponding simulated responses (solid orange lines) of (c, d) in-lake DOC concentration, (e, f) $K_{d\ PAR}$, and (g, h) $K_{d\ UV320}$.

Figure 3. Left panels: Comparison between observed (black points) and simulated (a) DOC surface values, (c) $K_{d\ PAR}$ surface values, and (e) $K_{d\ UV320}$ surface values at Lake Giles from the validation backcast period spanning 1998-2018 for the original model (blue line = fixed K_d) and its updated version (orange line = varying K_d). Shaded grey region indicates the calibration period. Right panels: Density plots of model residuals, centered on zero (solid vertical line) for simulated (b) DOC, (d) $K_{d\ PAR}$, and (f) $K_{d\ UV320}$ using the fixed model (dashed blue area with mean residual bias denoted by open triangle) and updated model (solid orange area with mean residual bias denoted by filled triangle).

Figure 4. Left panels: Comparison between observed (black points) and simulated (a) surface temperature and (c) deepwater temperature at Lake Giles from the validation backcast period

spanning 1998-2018 for the original model (blue line = fixed K_d) and its updated version (orange line = varying K_d). Shaded grey region indicates the calibration period. Right panels: Density plots of model residuals, centered on zero (solid vertical lines) for simulated (b) surface temperature and (d) deepwater temperature using the fixed model (dashed blue area with mean residual bias denoted by open triangle) and updated model (solid orange area with mean residual bias denoted by filled triangle).

Figure 5. Left panels: Comparison between observed (black points) and simulated (a) surface dissolved oxygen and (c) deepwater dissolved oxygen at Lake Giles from the validation backcast period spanning 1998-2018 for the original model (blue line = fixed K_d) and its updated version (orange line = varying K_d). Shaded grey region indicates the calibration period. Right panels: Density plots of model residuals, centered on zero (solid vertical lines) for simulated (b) surface dissolved oxygen and (d) deepwater dissolved oxygen using the fixed model (dashed blue area with mean residual bias denoted by open triangle) and updated model (solid orange area with mean residual bias denoted by filled triangle).

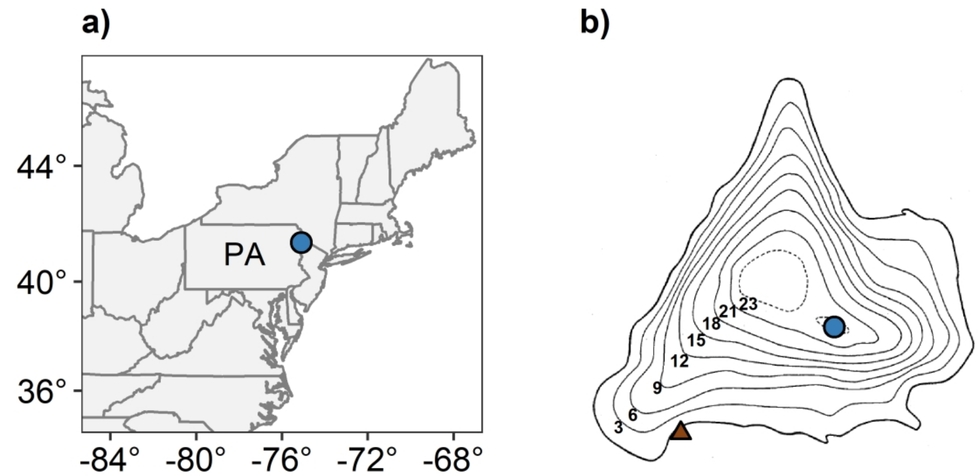

Figure 1. (a) Location of Lake Giles in northeastern Pennsylvania (blue point), and (b) bathymetric map of Lake Giles. Blue point in the center of the lake indicates the sampling location of manual samples and profiles and the mooring station of high-frequency sensors. Brown triangle in the lake shore indicates the approximate location of the ephemeral inflow stream.

127x63mm (600 x 600 DPI)

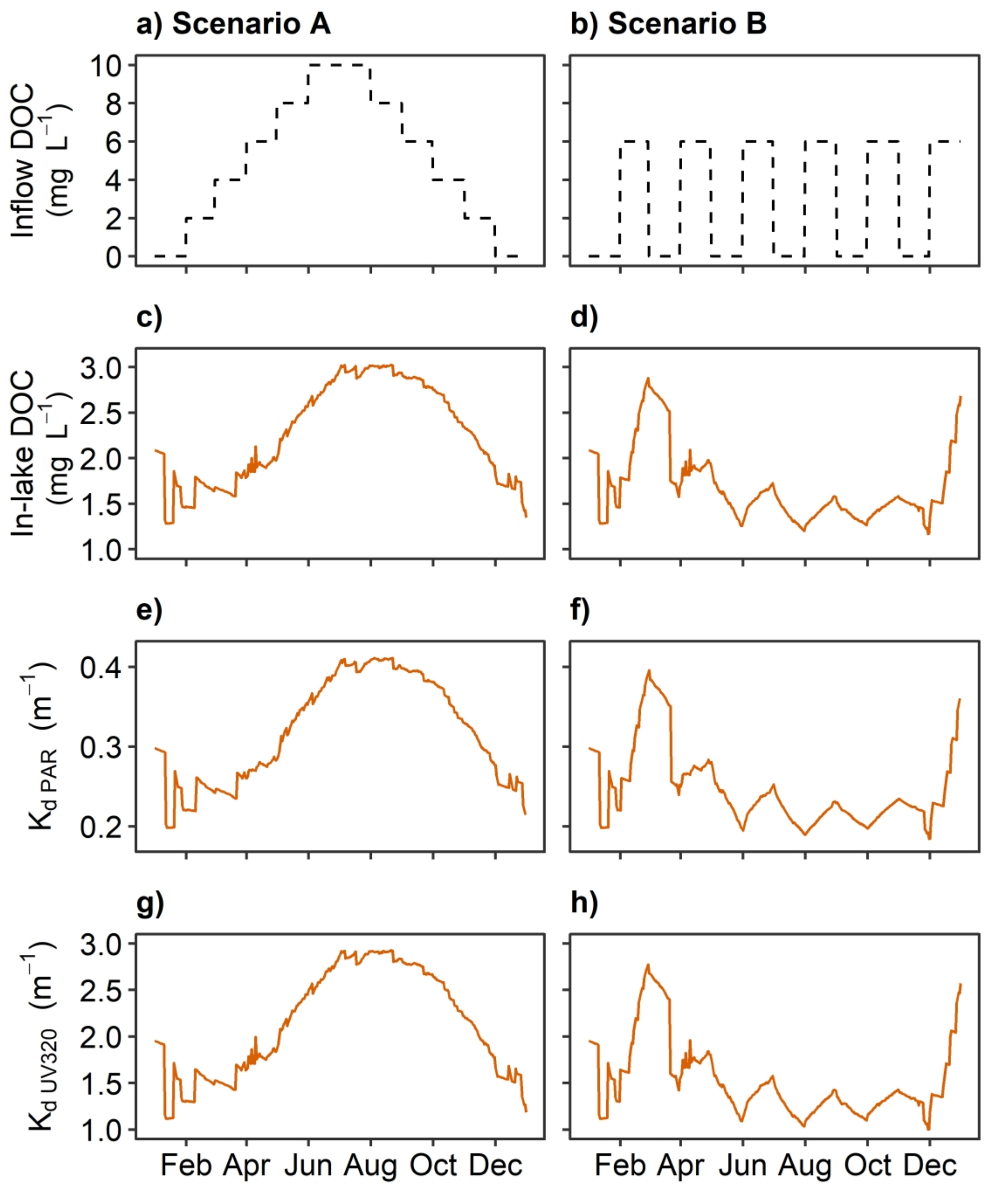

Figure 2. Scenarios A and B testing responsiveness to seasonal fluctuations of artificial time-series (black dashed lines) of (a, b) inflow DOC concentration, and the corresponding simulated responses (solid orange lines) of (c, d) in-lake DOC concentration, (e, f) Kd PAR, and (g, h) Kd UV320.

127x152mm (600 x 600 DPI)

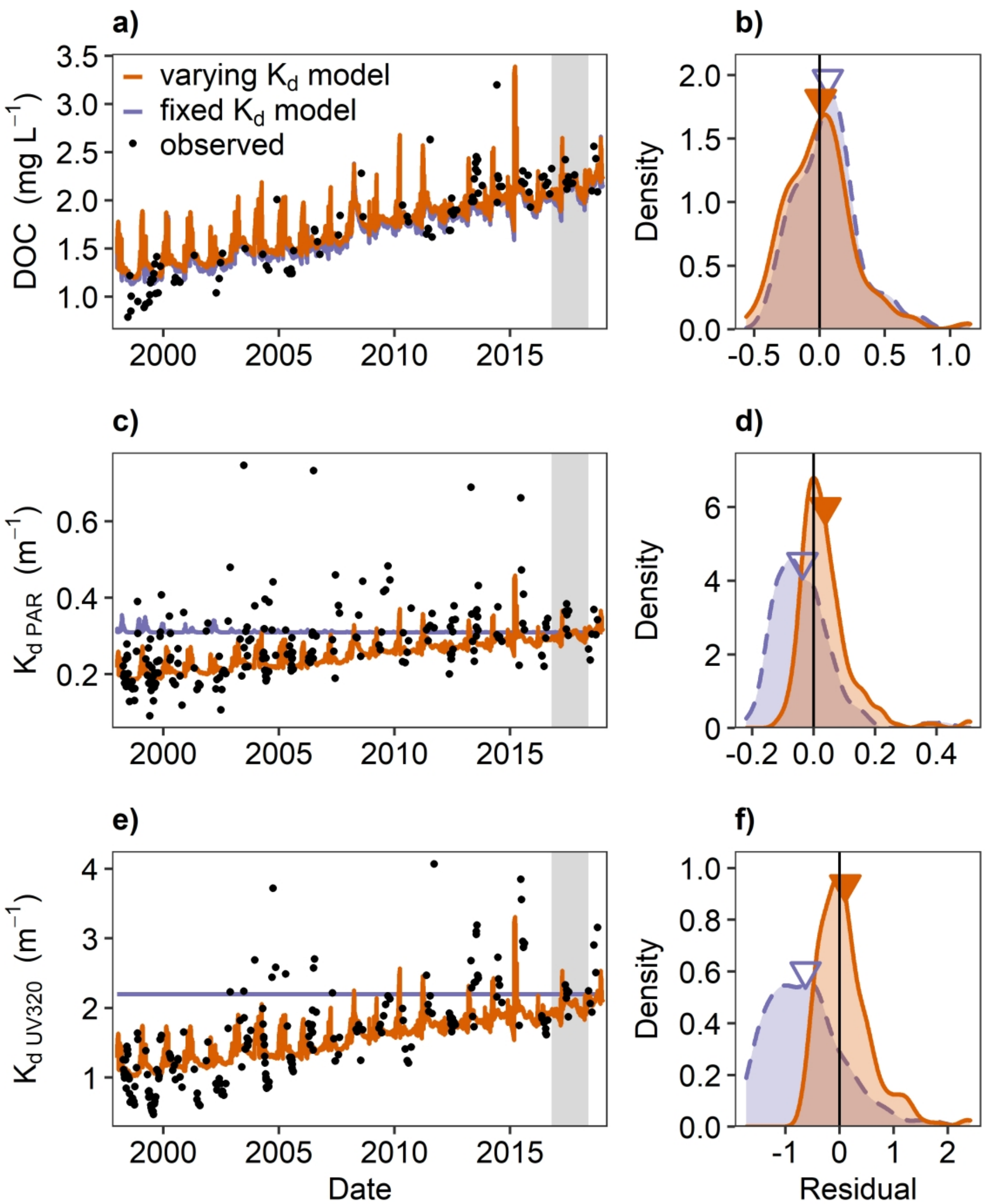

Figure 3. Left panels: Comparison between observed (black points) and simulated (a) DOC surface values, (c) Kd PAR surface values, and (e) Kd UV320 surface values at Lake Giles from the validation backcast period spanning 1998-2018 for the original model (blue line = fixed Kd) and its updated version (orange line = varying Kd). Shaded grey region indicates the calibration period. Right panels: Density plots of model residuals, centered on zero (solid vertical line) for simulated (b) DOC, (d) Kd PAR, and (f) Kd UV320 using the fixed model (dashed blue area with mean residual bias denoted by open triangle) and updated model (solid orange area with mean residual bias denoted by filled triangle).

127x152mm (600 x 600 DPI)

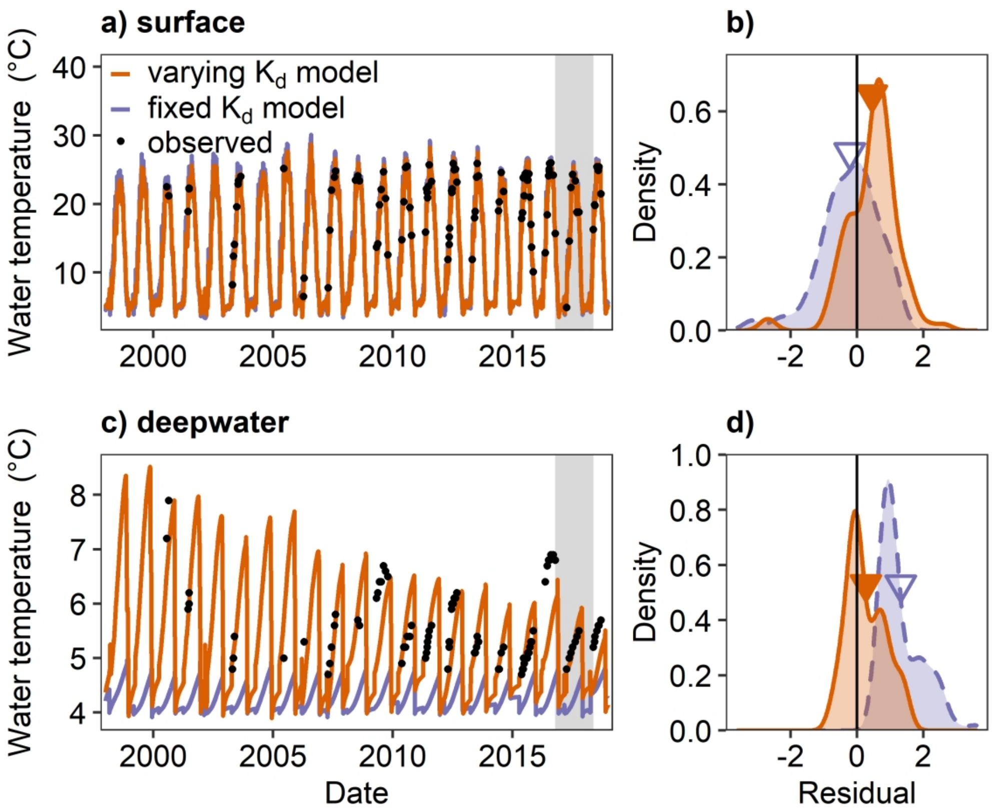

Figure 4. Left panels: Comparison between observed (black points) and simulated (a) surface temperature and (c) deepwater temperature at Lake Giles from the validation backcast period spanning 1998-2018 for the original model (blue line = fixed Kd) and its updated version (orange line = varying Kd). Shaded grey region indicates the calibration period. Right panels: Density plots of model residuals, centered on zero (solid vertical lines) for simulated (b) surface temperature and (d) deepwater temperature using the fixed model (dashed blue area with mean residual bias denoted by open triangle) and updated model (solid orange area with mean residual bias denoted by filled triangle).

127x101mm (600 x 600 DPI)

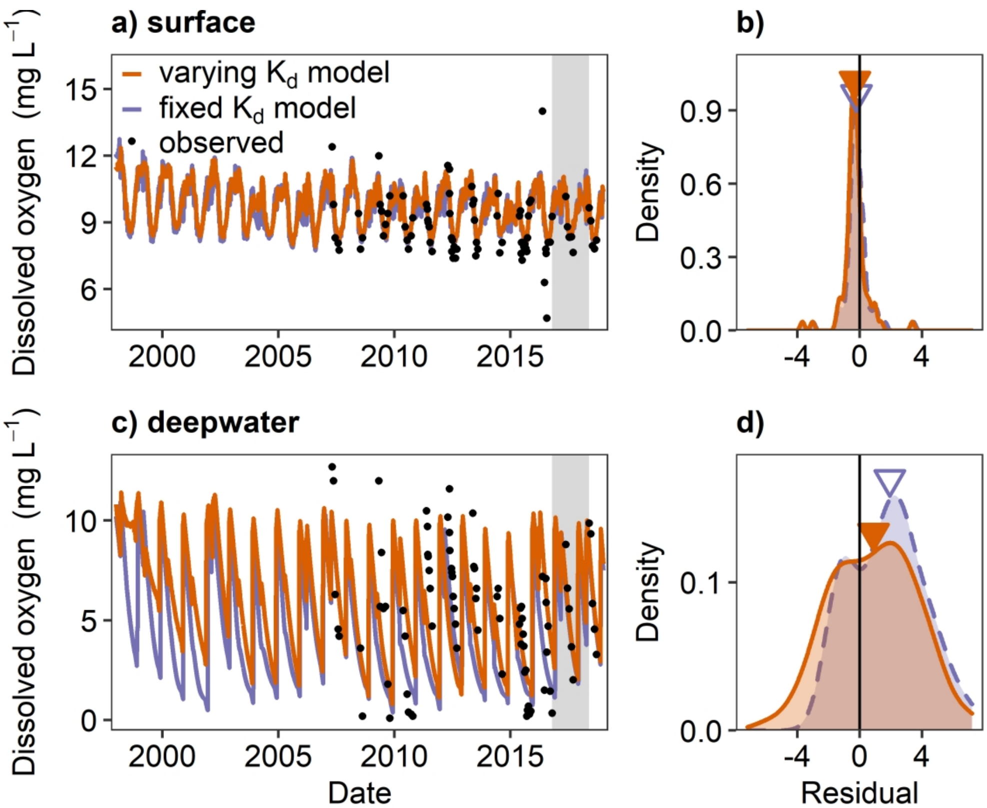

Figure 5. Left panels: Comparison between observed (black points) and simulated (a) surface dissolved oxygen and (c) deepwater dissolved oxygen at Lake Giles from the validation backcast period spanning 1998-2018 for the original model (blue line = fixed Kd) and its updated version (orange line = varying Kd). Shaded grey region indicates the calibration period. Right panels: Density plots of model residuals, centered on zero (solid vertical lines) for simulated (b) surface dissolved oxygen and (d) deepwater dissolved oxygen using the fixed model (dashed blue area with mean residual bias denoted by open triangle) and updated model (solid orange area with mean residual bias denoted by filled triangle).

127x101mm (600 x 600 DPI)

Supplemental Information

Attenuation of photosynthetically active radiation and ultraviolet light in response to changing dissolved organic carbon in browning lakes: Modelling and parametrization

Authors & Affiliations:

Rachel M. Pilla[1*] (pillarm@miamioh.edu; ORCID 0000-0001-9156-9486)

Raoul-Marie Couture[2] (raoul.couture@chm.ulaval.ca; ORCID 0000-0003-4940-3372)

[1]Department of Biology, Miami University, Oxford, Ohio, USA

[2]Centre for Northern Studies (CEN), Takuvik Joint International Laboratory, and Department of Chemistry, Université Laval, Quebec City, QC, Canada

[*]corresponding author

Contents:

Summary of model description:

Three key processes are responsible for DOC processing in the model: microbial metabolism, photodegradation, and flocculation and subsequent sinking. Key parameters are given in Table S1. Microbial metabolism, or bacterial decay of organic matter (OM), assumes three pools (e.g., a 3G approach to OM degradation; Arndt et al. 2013) composed of compound classes characterized by a specific rate constant parametrizing bacterial mineralization. These pools are OM_a, labile organic matter originating from autochthonous biomass, i.e., phytoplankton; OM_b, semi-labile organic matter originating from allochthonous carbon; and OM_c, the non-reactive fraction. Each pool contains a particulate (POC) and a dissolved (DOC) fraction. In this application at Lake Giles, we focus exclusively on DOC and POC part of the semi-labile OM_b pool. The rate for allochthonous DOC mineralization via oxic metabolism, for example, is formulated as follows:

$$R_{METAB} = k_{DOC} \times \theta^{T-T\_ref} \times [DOC]_i \times \frac{[O_2]}{K^m_{O_2} + [O_2]}$$

where R_{METAB} (mg C m^{-3} d^{-1}) is function of the rate constant k_{DOC} (d^{-1}), [DOC] are the DOC concentrations (μg m^{-3}), $[O_2]$ are the oxygen concentrations (mg m^{-3}), K^m is the half-saturation constant (mg m^{-3}), and θ_{OM} is the temperature adjustment coefficient. Decomposition is thus assumed to have temperature dependence similar to that of the phytoplankton processes.

The rate of DOC photodegradation (R_{PHOTO}) is calculated by considering light absorption by water, phytoplankton, and chromophoric DOC, as well as light scattering and shading. This allows calculation of light attenuation and the rate of DOC photodegradation by photons (R_{PHOTO}, mg C d^{-1}) as follows (Saloranta and Andersen 2007):

$$R_{PHOTO} = -oc\_DOC \times qy\_DOC \times f\_par \times \frac{1}{e\_par} \times 86{,}400 \times Q_{sw} \times Attn\_z$$

where oc_DOC is the optical cross-section of DOC (m^2 mg^{-1}), qy_DOC is the quantum yield (mg mol quanta^{-1}), f_par is the fraction of PAR radiation, e_par the average energy of PAR photons (J mol^{-1}), Q_{sw} the incoming solar radiation flux at the surface (J s^{-1} m^{-2}), and Attn_z the model calculated light attenuation depth profile. Q_{sw} is calculated during the fractions of day when the sun angle is above and below a preset threshold value (currently 15°). MyLake relies on the MATLAB Air-Sea Toolbox (http://woodshole.er.usgs.gov/operations/sea-mat/) to calculate radiative flux and astronomical variables needed to calculate short- and long-wave radiation.

Finally, the removal of DOC by flocculation (R_{FLOCC}) yields POC suspended in the water column. R_{FLOCC} is calculated by using a rate constant for flocculation. R_{FLOCC} was parametrized according to de Wit et al. (2018) who adjusted its value to reproduce the sediment carbon mass accumulation rate (mg C m^{-2} yr^{-1}) obtained via dating at the deepest point of the oligotrophic Lake Langtjern, Norway. We assume that flocculation is the dominant pathway for sediment formation, which is a reasonable assumption in oligotrophic humic lakes (von Wachenfeldt and Tranvik 2008). In addition to advective transport, POC is subjected to sinking towards the sediment-water interface by a settling velocity w (m d^{-1}). The key parameters modulating the DOC-dependent flocculation rate (mg m^{-2} yr^{-1}) and the sinking rate of flocculates (m d^{-1}) were bound by literature values (Burban et al. 1990; von Wachenfeldt and Tranvik 2008). The sinking rate was adjusted to 1.6 m d^{-1} by de Wit et al. (2018). This value falls within the range of 0.1 to 3 m d^{-1} calculated for particle sizes ranging from 0.45 μm (i.e., defined as particulate OC according to filter size) to 45 μm (Burban et al. 1990).

Table S1. Key parameters related to the MyLake model calibration and its sediment module. The three new parameters are in bold under “Light attenuation” parameters. Parameter type indicates literature values (L) or constrained (C) with the model after calibration.

Parameter	Value	Unit	Type	Definition	Reference
Metabolism					
Cx1:Ny1:Pz1	112:20:1	-	L	Pool 1 – stoichiometry	Canavan et al. 2006
Cx2:Ny2:Pz2	200:20:1	-	L	Pool 2 – stoichiometry	Canavan et al. 2006
$K^{m}_{O_2}$	1.23×10^{-2}	µmol cm^{-3}	L	Respiration half-sat.	Couture et al. 2016
k_{DOC1}	not used	yr^{-1}	L	OM1 deg. rate cst.	de Wit et al. 2018
k_{DOC2}	0.84	yr^{-1}	C	OM2 deg. rate cst.	
accel	90	-	C	Oxic respiration scaling factor	
Q10_wc	0.72	-	C	Metabolism adjustment for T	Kiuri et al. 2019
T_ref_wc	9.8	-	C	Threshold for T effect	Kiuri et al. 2019
Flocculation					
d_floc	0.15	m^{-2} d^{-1}	C, L	Floc. rate	de Wit et al. 2018
w	0.84	m d^{-1}	L	Floc. sinking velocity	Burban et al. 1990
Photodegradation					
qy_DOC	0.007	mg mol $quanta^{-1}$	L	Quantum yield	Saloranta and Andersen 2007
oc_DOC	0.040	m^2 mg^{-1}	L	Optical cross section	Saloranta and Andersen 2007
e_par	240800	J mol^{-1}	L	Energy of PAR photon	Saloranta and Andersen 2007
Sediment module					
φ	0.85-0.98	cm^3 cm^{-3}	L	Porosity	de Wit et al. 2018
D_B	0	cm^2 yr^{-1}	L	Bioturbation coefficient	Couture et al. 2016
α	14.4	yr^{-1}	L	Bioirrigation constant	Couture et al. 2016
Inflow scaling					
I_scDOC	0.77	-	C	Inflow DOC scaling factor	
I_scO	1.00	-	C	Inflow DO scaling factor	
I_scT	9.79	ºC	C	Inflow T scaling coeficient	
I_scPOC	2.83	-	C	Inflow POC scaling factor	
I_scV	5.0	-	C	Inflow V scaling factor	
Light attenuation					
βDOC	**1.0×10^{-4}**	**m^2 mg^{-1}**	**C**	**Optical cross-section of DOC for PAR**	
βChl	6.0×10^{-4}	m^2 mg^{-1}	C	Optical cross-section of chlorophyll	
K_{d0}’	**-0.22**	**m^{-1}**	**C**	**Background $UV_{320\ nm}$ attenuation of water**	
β’DOC	**1.04**	**m^2 mg^{-1}**	**C**	**Optical cross-section of DOC for $UV_{320\ nm}$**	
ε_0	0.07	m^{-1}	C	Non-PAR light extinction coefficient of water	
$\hat{\varepsilon}_0$	0.04	m^{-1}	C	PAR light extinction coefficient of water	
Physical parameters					
α_{snow}	0.56	-	C	Melting snow albedo	
α_{ice}	0.23	-	C	Melting ice albedo	
W_{str}	0.04	-	C	Wind sheltering coefficient	
a_k	1.0×10^{-3}	-	C	Open water diffusion parameter	
a_k	1.0×10^{-4}	-	C	Ice covered diffusion parameter	

Figure S1. Daily meteorological input data used in the model for (a) air temperature, (b) global shortwave radiation, (c) precipitation, (d) wind speed, (e) relative humidity, and (f) air pressure.

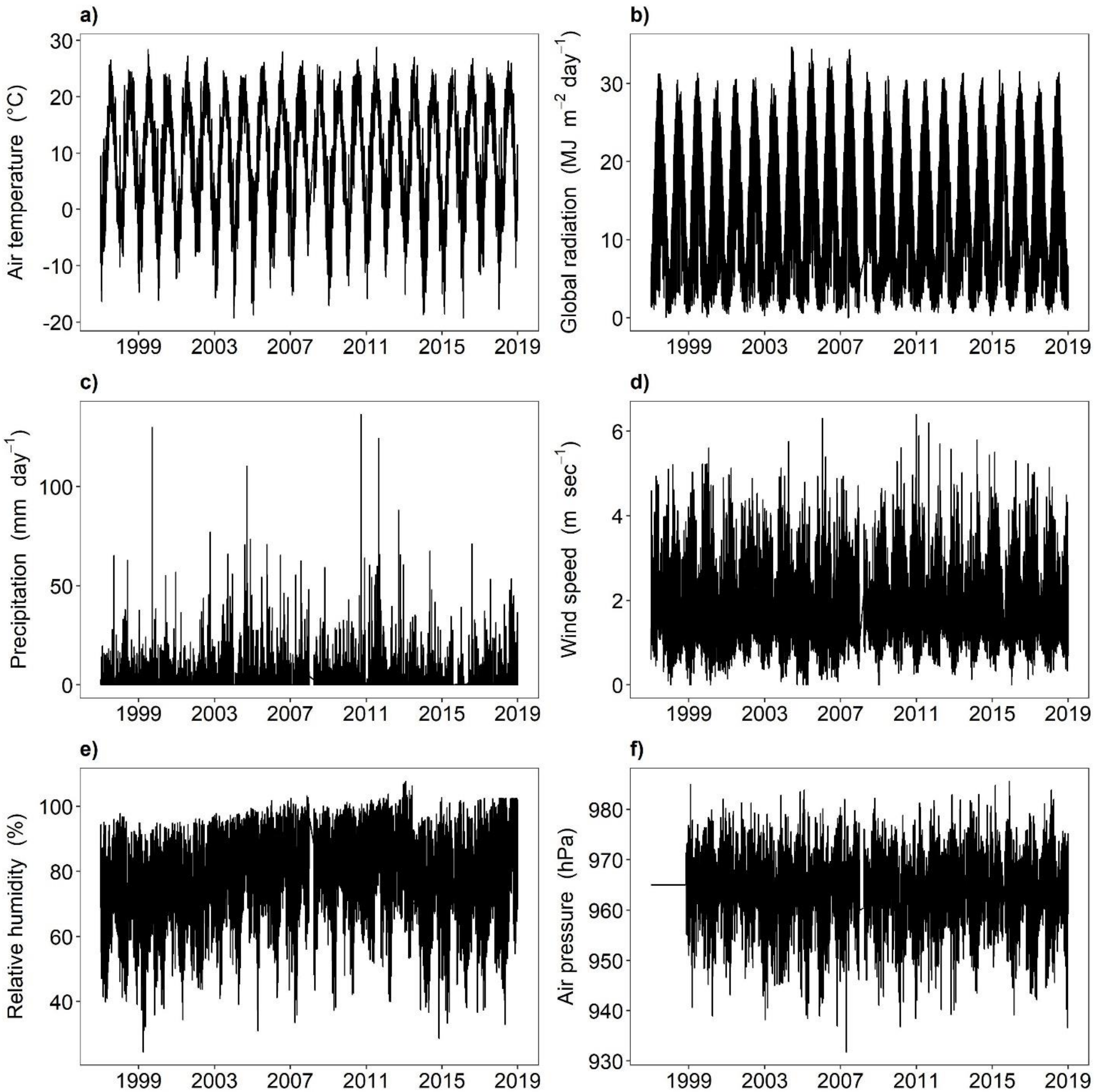

Figure S2. Daily estimated inflow input data used in the model for (a) inflow volume, (b) inflow temperature, (c) inflow dissolved oxygen, (d) inflow dissolved organic carbon, and (e) inflow particulate organic carbon.

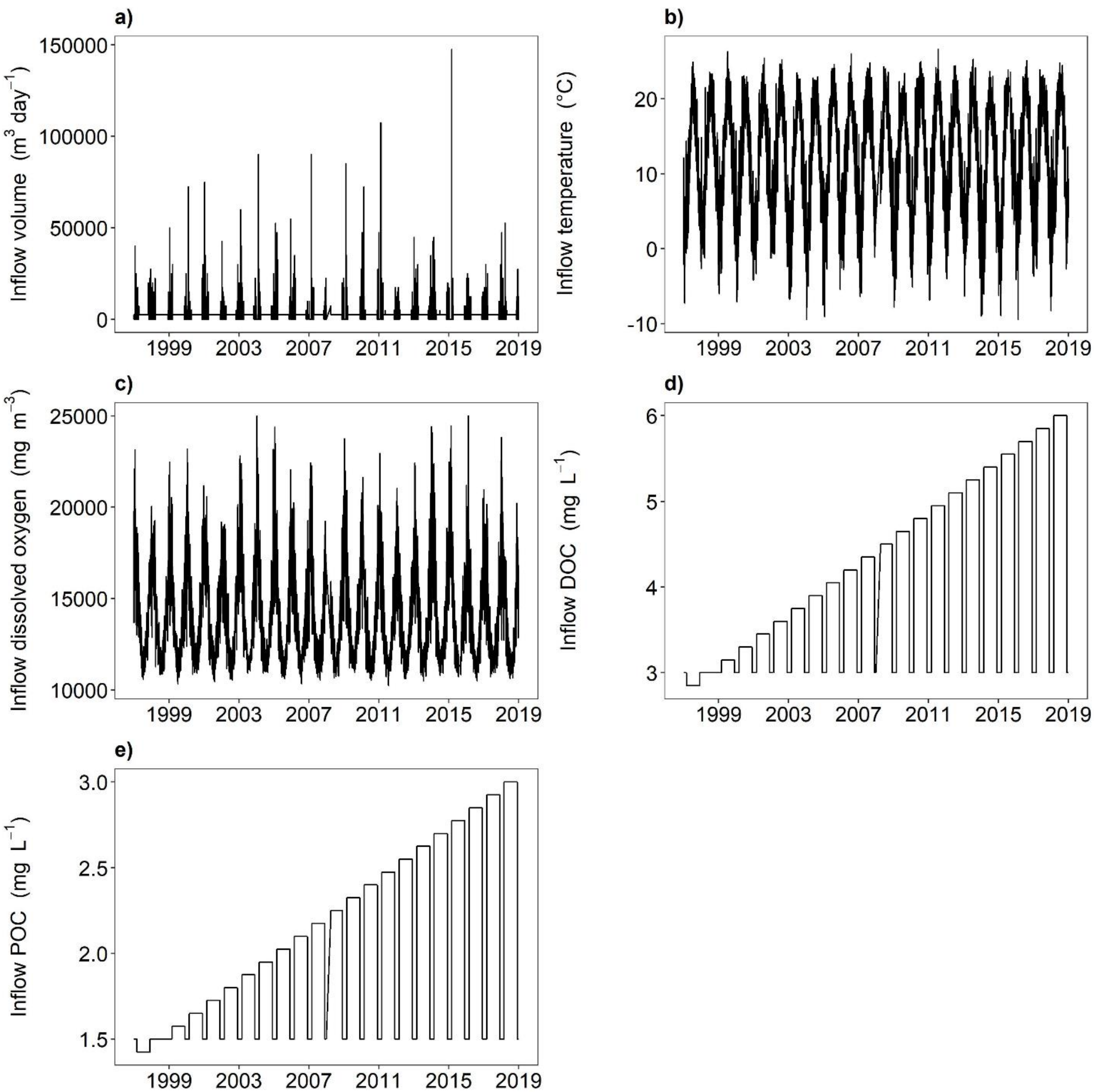

Figure S3. Target diagram of the variables and depths included in the calibration periods spanning 2016-2018. Outer black circle spans values of 1.0 for both normalized bias and normalized RMSD', and inner grey circle spans values of 0.75 for both. Symbol shape represents one of the five state variables included in the calibration routine, and color represents depth (red = shallow depths, blue = deep depths).

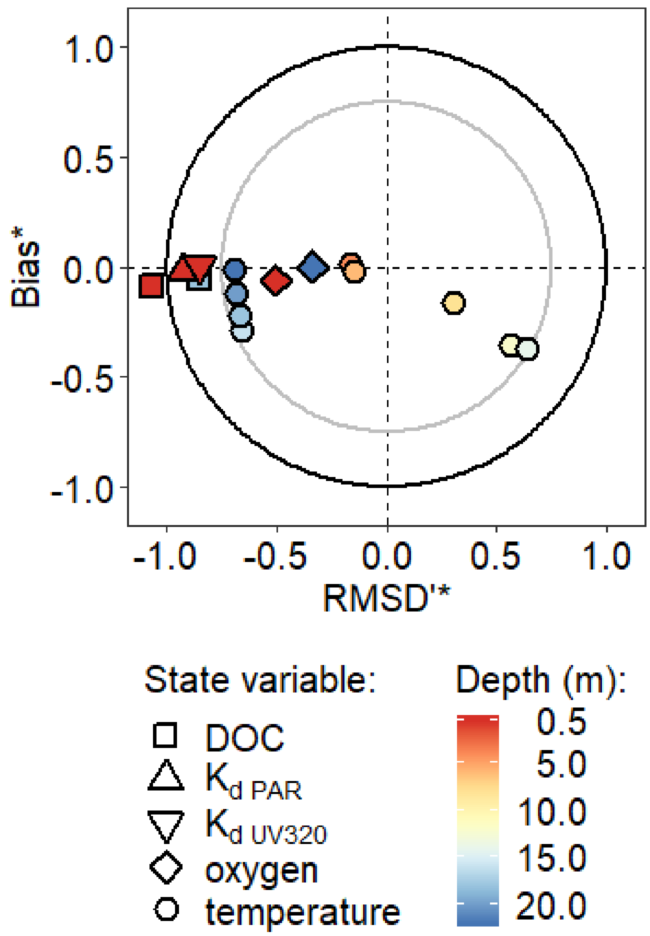

74 **Figure S4.** Modelled (blue line) vs. observed (black points) DOC concentration at Lake Giles
75 from the calibration period spanning 2016-2018. Top panel is surface measurements at 0.5 m,
76 and bottom panel is deepwater measurements from 18 m.

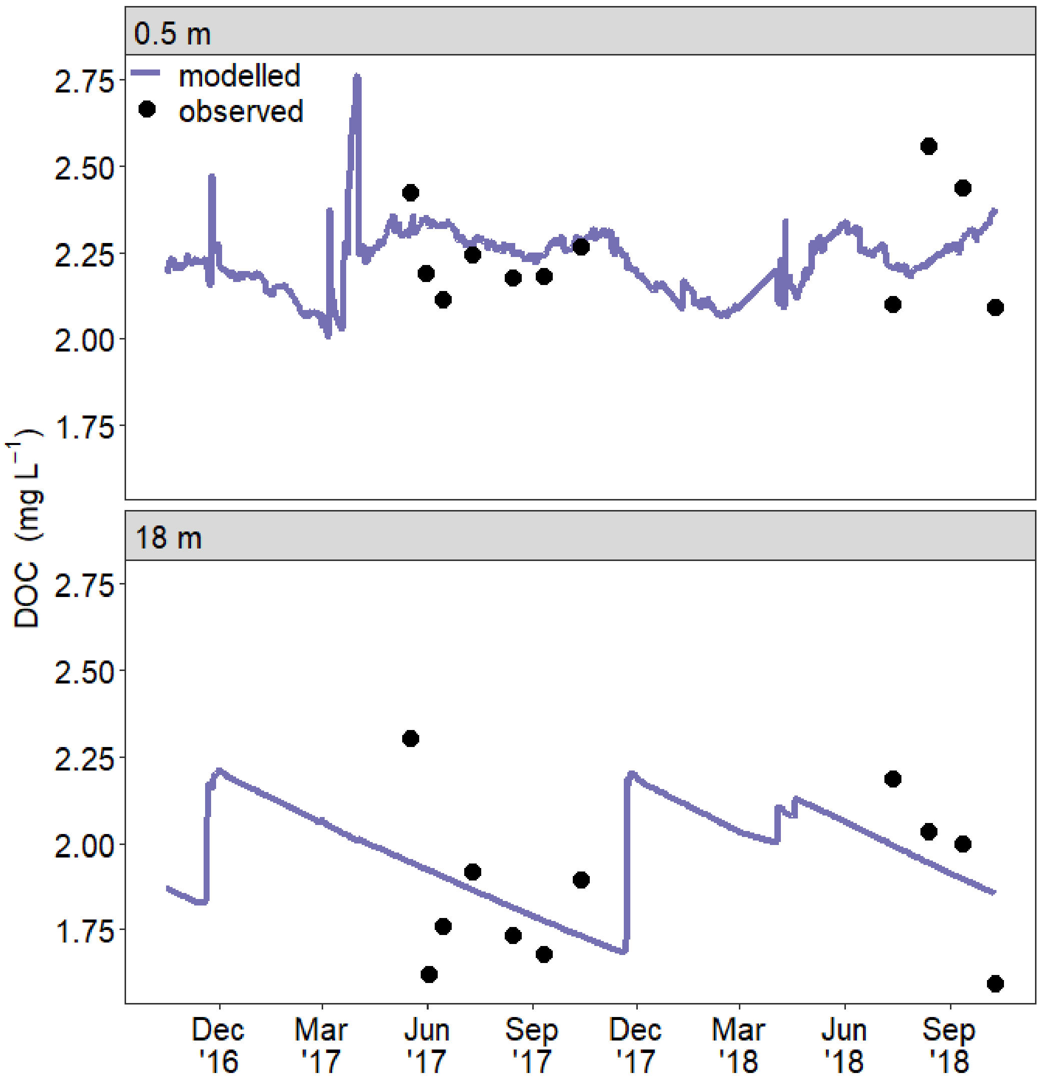

Figure S5. Modelled (blue line) vs. observed (black points) of $K_{d\ PAR}$ surface values (top panel) and $K_{d\ UV320}$ surface values (bottom panel) at Lake Giles from the calibration period spanning 2016-2018.

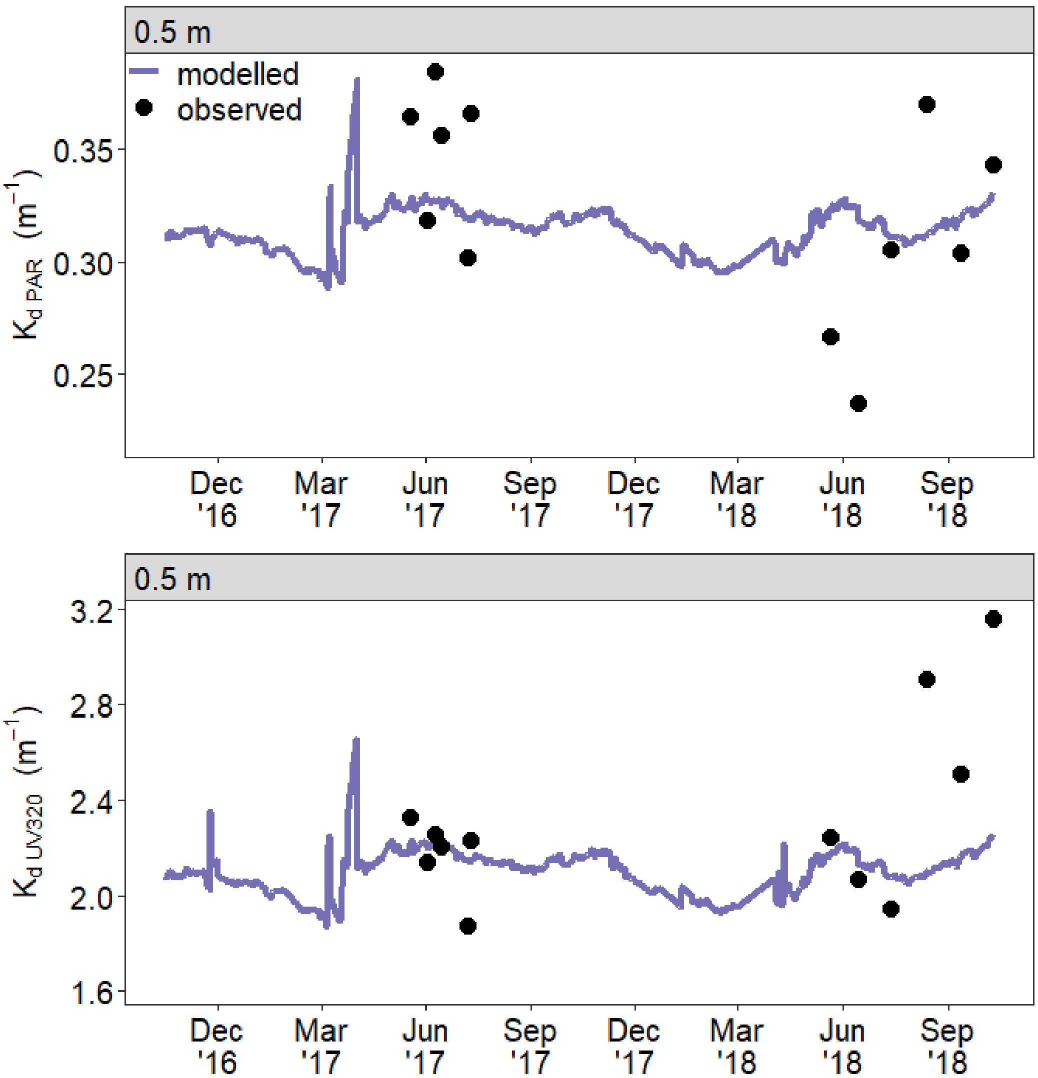

Figure S6. Modelled (blue line) vs. observed manual (black points) and observed high-frequency (grey diamonds) water temperature at Lake Giles from the calibration period spanning 2016-2018. Each panel represents a different depth from 4 m through 22 m.

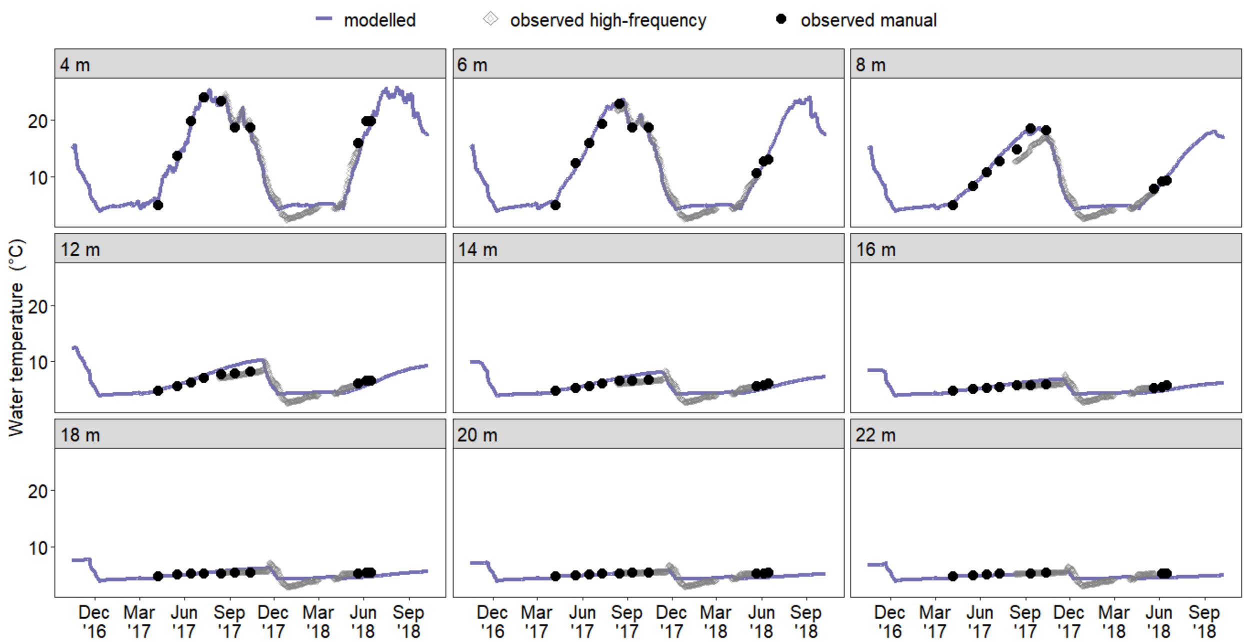

Figure S7. Modelled (blue line) vs. observed manual (black points) and observed high-frequency (grey diamonds) dissolved oxygen at Lake Giles from the calibration period spanning 2016-2018. Top panel is surface measurements at 0.5 m, and bottom panel is deepwater measurements from 22 m. Note that the dissolved oxygen under ice during early 2018 was poorly captured in the model.

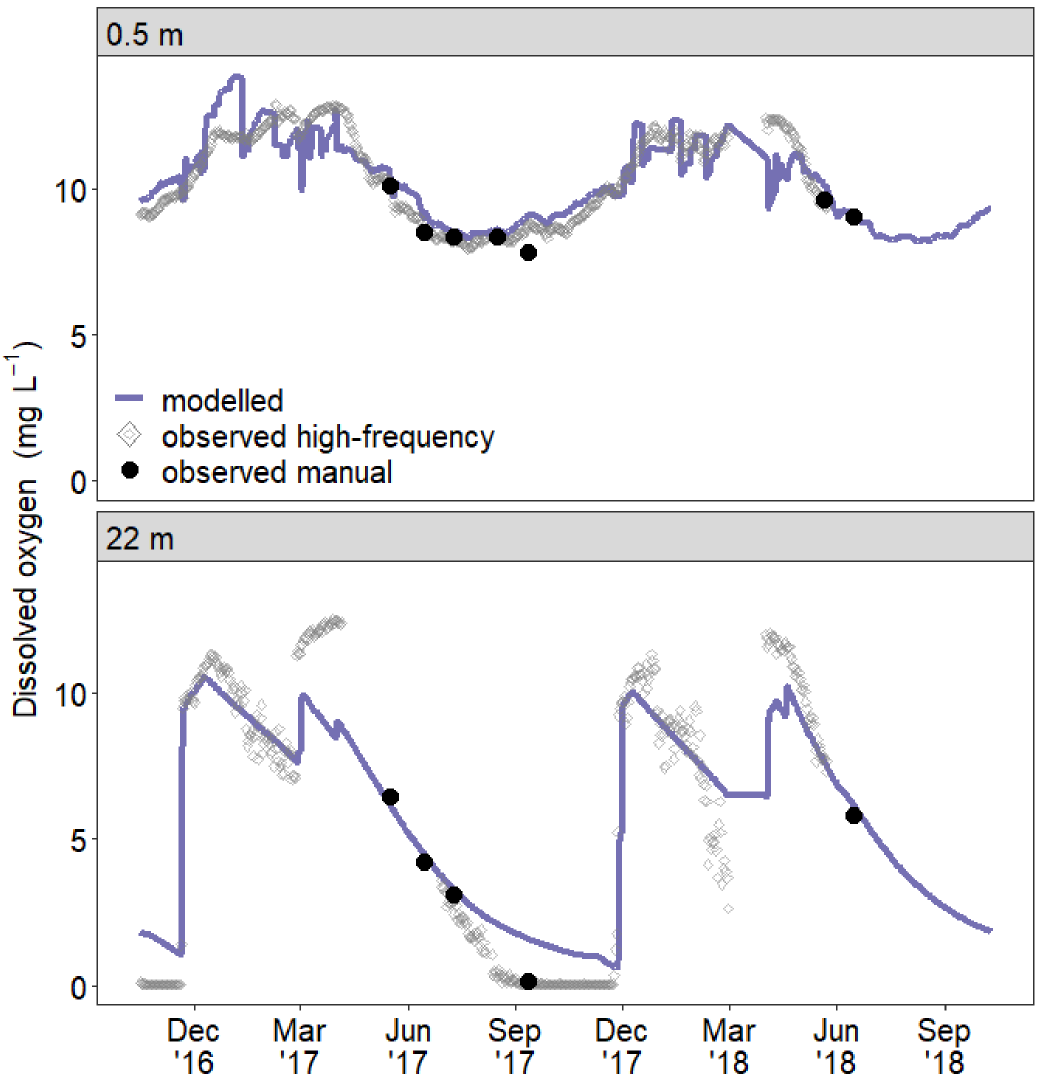

References:

Arndt, S., B. B. Jørgensen, D. E. LaRowe, J. J. Middelburg, R. D. Pancost, and P. Regnier. 2013. Quantifying the degradation of organic matter in marine sediments: A review and synthesis. Earth-Science Reviews doi:10.1016/j.earscirev.2013.02.008

Burban, P.-Y., Y.-J. Xu, J. McNeil, and W. Lick. 1990. Settling speeds of floes in fresh water and seawater. J. Geophys. Res.: Oceans doi:10.1029/JC095iC10p18213

Canavan, R. W., C. P. Slomp, P. Jourabchi, P. Van Cappellen, A. M Laverman, and G. A. van den Berg. 2006. Organic matter mineralization in sediment of a coastal freshwater lake and response to salinization. Geochim. Cosmochim. Acta doi:10.1016/j.gca.2006.03.012

Couture, R.-M., R. Fischer, P. Van Cappellen, and C. Gobeil. 2016. Non-steady state diagenesis of organic and inorganic sulfur in lake sediments. Geochim. Cosmochim. Acta doi:10.1016/j.gca.2016.08.029

de Wit, H. A., R.-M. Couture, L. Jackson-Blake, M. N. Futter, K. Austnes, J.-L. Guerrero, and Y. Lin. 2018. Pipe or chimneys? For carbon cycling in small boreal lakes, preciptiation matters most. Limnol. Oceanogr. Lett. doi:10.1002/lol2.10077

Kiuru, P., Ojala, A., Mammarella, I., Heiskanen, J., Erkkilä, K.M., Miettinen, H., Vesala, T. and Huttula, T. 2019. Applicability and consequences of the integration of alternative models for CO_2 transfer velocity into a process-based lake model. Biogeosciences 16: 3297-3317.

Saloranta, T. M. and T. Andersen. 2007. MyLake—A multi-year lake simulation model code suitable for uncertainty and sensitivity analysis simulations. Ecol. Modell. 207: 45-60.

von Wachenfeldt, E. and Tranvik, L. 2008. Sedimentation in Boreal Lakes: the role of flocculation of allochthonous dissolved organic matter in the water column. Ecosystems doi:10.1007/s10021-008-9162-z